Contract number: 4000148450

MOMO-NBS

Scientific Methodology Strategy
Version 1.1

UNIVERSITÀ DI PAVIA

BROCKMANN CONSULT

KTH VETENSKAP OCH KONST

DLR Deutsches Zentrum für Luft- und Raumfahrt

Authors: The MOMO-NBS team
Date: 11 April 2026

Approval/Signature field

Approved by	Contractor	Customer
Name:	P. Gamba	Sophie Hebden
Organisation:	UNIPV	ESA
Position:	Prime Representative	Technical Officer
Date:		
Signature:		

Change Record

Issue	Date	Section	Change
V0.1	18/03/2026	All	Draft with section titles and assignments
V0.2	27/03/2026	All	Draft with all section
V0.3	11/04/2026	All	Semi-final version
V1.0	17/04/2026	All	Version submitted to ESA
V1.1	10/06/2026	All	Revised version after ESA comments

Scope of this document

This document provides the outputs of WP2 “Methods development, which aims at co-designing with the stakeholders the analysis methodologies suited to the overarching scientific topics and their requirements as obtained by the work in WP1 “State of the art, knowledge gaps and user needs”. Accordingly, this document starts from the outputs of WP1, namely deliverables D1.2 “Science Requirements Document” and D1.3 “Dataset Inventory Document”.

Table of Contents

1. List of acronyms

Acronym	Definition
AI	Artificial Intelligence
AOD	Aerosol Optical Depth
BF	Building footprint
BGI	Blue-Green Infrastructure
DLR	German Aerospace Center
EO	Earth Observation
ECV	Essential Climate Variable
GHS	Global Human Settlement
GHSL	Global Human Settlement Layer
GIS	Geographic Information System
GSI	Green Stormwater Infrastructure
JRC	Joint Research Center
LST	Land Surface Temperature
LCZ	Local Climate Zones
NBS	Nature-Based Solutions
RF	Random Forest
SUHI	Surface Urban Heat Island
UCBD	Urban Centre Database
UNIPV	University of Pavia
WSF	World Settlement Footprint

2. Introduction

This report presents the results of the activities of WP2 and is structured according to the tasks that are mentioned in the MOMO-NBS Implementation proposal document, i.e., a critical assessment of all relevant datasets and their uncertainties collected in WP1, a report about the procedures used for city selections in the global and local study, a report about the feasibility studies initially performed to ensure that the methodology is appropriate, a report about the procedures used to tailor the observational data to be used in the studies, the assessment of the added value of EO to the science challenge, and, finally, an analysis of risks to successfully achieving the scientific objectives as well as of the approaches for the mitigation of these risks.

3. Critical assessment of all relevant datasets and their uncertainties collected in WP1

This section builds on two complementary inputs. The first is the dataset inventory and evaluation framework established in D1.3, which provides harmonized metadata on record length, temporal resolution, spatial resolution, accessibility, and uncertainty information for the selected ECV products. The second one is the morphology–ECV screening, which supports the identification of the variables most relevant for analyzing the links between urban morphology, Nature-Based Solutions (NBS), and climate effects. In this context, the DLR scoring scheme is used as an existing observation-capacity framework rather than as a universal or definitive ranking of datasets. While this framework is well suited to the global-study perspective, the local study requires an additional interpretation focused on whether a given product can resolve morphology-sensitive differences within the city and support the attribution of NBS-related effects.

3.1. The D1.3 scoring framework and its implications for the global/local studies

The evaluation scheme established in D1.3 clarifies the rationale behind the spatial and temporal scores reported in the dataset inventory. Spatial scores are linked to the observational scale of each product: score 5 refers to object-level

detail, score 4 to street- or parcel-scale mapping, score 3 to neighborhood-scale patterns, score 2 to district- or meso-scale contrasts, and score 1 to regional or background-climate context. Record scores are linked to record length: score 5 refers to climatological records of at least 30 years, score 4 to decadal monitoring, score 3 to multi-year variability analysis, score 2 to seasonal-to-interannual assessment, and score 1 to event-based or diurnal monitoring only. The scoring matrix then combines these two dimensions into an indicative statement of observational capacity.

This framework is methodologically robust and particularly valuable for comparing datasets in a harmonized way across variables and cities. At the same time, its logic is primarily aligned with the needs of broad-scale and long-term assessment, and therefore tends to favor products that are stable, continuous, and globally available, even when their spatial support is too coarse for intra-urban interpretation. For this reason, the present section distinguishes suitability explicitly between the global study and the local study. In practice, products with score profiles such as 1/5 or 1/4 may still be highly valuable as contextual climate baselines, whereas products with profiles such as 3/3 or 4/3 may be more informative for detecting neighborhood-scale contrasts associated with urban form, land cover, or NBS-related effects.

Table 3.1. DLR scoring foundations and how they should be read for MOMO-NBS.

Dimension	Score	Threshold	Observable capacity in D1.3scheme	Implications for MOMO local study
Spatial	5	≤ 1 m	Object-level; individual features can be resolved with minimal spectral mixing.	Excellent for object-based mapping, but rarely available for the ECV products in the inventory.
Spatial	4	1-30 m	Street/parcel scale; major urban features and local contrasts can be separated.	Best range for direct local-study interpretation of morphology and many NBS effects.
Spatial	3	30-100 m	Neighborhood scale; district patterns are visible but individual buildings are lost.	Still useful for local study, especially for neighborhood contrasts and urban gradients.
Spatial	2	100-500 m	District/meso-scale; signals are strongly mixed within the pixel.	Useful for broad intra-urban contrasts, but insufficient for small interventions.
Spatial	1	> 500 m	Regional/background climate; the city is effectively represented as	Mainly contextual for local study; robust for global

			a point or small cluster of pixels.	comparison but weak for direct attribution.
Record	5	≥ 30 years	Climate-normal perspective; supports robust trend and recurrence analysis.	Ideal for global baselines and long-term framing.
Record	4	10-29 years	Decadal monitoring and change detection.	Strong support for trend analysis, but spatial suitability still depends on pixel size.
Record	3	5-<10 years	Multi-year variability assessment.	Often a good compromise when finer-resolution products exist.
Record	2	1-<5 years	Seasonal-to-interannual assessment.	Useful for recent local mapping, but not for climatological interpretation.
Record	1	< 1 year	Event-scale or diurnal monitoring only.	Suitable only for short-term experiments or episodic interpretation.

3.2. Prioritized ECVs from the morphology-NBS perspective

The complementary WP1 screening does not replace the DLR inventory; rather, filters it according to the specific requirements of the local study. In WP1, 52% of the reviewed 2D/3D morphology studies focused on heat-related hazards such as urban heat islands and heatwaves, and a smaller share addressed air-quality impacts. This is the main reason why, in WP2, we give priority to ECVs that are directly relevant for heat and air-quality analysis On this basis, the prioritized subset of ECVs comprises Land Surface Temperature (LST), albedo, greenhouse gases, aerosol properties, surface radiation budget, above-ground biomass and vegetation-related proxies, land cover, and precipitation. These variables have direct or indirect link to target NBS under MOMO-NBS scope and the linked morphologies such as urban density, building height, surface materials, street-canyon configuration, vegetation presence, imperviousness, and the broader morphology of the territory.

This prioritization also helps clarify the different roles of ECVs within the overall assessment framework. LST represents the principal climate-response variable for urban heat and heat-mitigation analyses. Land cover and vegetation-related products are essential for characterizing the surfaces and NBS elements that may

explain thermal differences across the urban fabric. Albedo and surface radiation budget contribute to the interpretation of energy-balance processes and material-related effects. Aerosols, greenhouse gases, and precipitation remain relevant mainly as contextual forcing variables, even where they are scientifically important for the broader rationale of the project.

Table 3.2. Priority ECV subset and its relevance for morphology-sensitive local analyses.

ECV family	Main local-study role	Main morphology/NBS links	Indicative scale represented in the inventory	Operational role
Land Surface Temperature	Primary climate-response variable	Urban density, building height, materials, vegetation/NBS presence	From 70 m to 1 km	Core variable
Land Cover	Primary surface descriptor	Imperviousness, land consumption, green/grey surface patterns	From 10 m to 300 m	Core variable
Above-ground biomass / vegetation proxies	Vegetation condition and canopy support	Vegetation presence, NBS presence, canopy effects	From 100 m to 1 km	Secondary support
Albedo	Material and energy-balance interpretation	Materials, reflective behaviour, NBS presence	From 300 m to 1 km	Secondary support
Surface Radiation Budget	Background energy forcing	Urban density, street canyon, materials, NBS presence	From 5.5 km to 25 km	Contextual variable
Aerosol Properties	Air-quality and atmospheric context	Urban density, street canyon, NBS presence	From 1 km to 110 km	Contextual variable
Greenhouse Gases	Urban emissions context	Urban density, street canyon, plot shape, NBS presence	From 2.25 km to 500 km	Contextual variable
Precipitation	Hydro-climatic forcing	Territorial morphology, runoff context, flood-related sensitivity	From 5.5 km to 10 km	Contextual variable

3.3. Critical assessment of the prioritized ECVs and their uncertainties

The inventory shows that the prioritized variables are all scientifically relevant, although their suitability differs substantially when considering the objectives of the global and local studies. For the local study, the most robust combination is LST together with land cover. LST illustrates the central trade-off particularly well: the inventory includes both a long-record, coarse-resolution product (CCI LST, 1

km, 31 years; spatial score 1, record score 5) and a much finer-resolution but shorter-record product (ECOSTRESS, 70 m, 8 years; spatial score 3, record score 3). Land cover provides the clearest bridge between global and local requirements, as the inventory combines long-term coarser products with several higher-resolution products such as HRLC 10/30 m, ESA WorldCover 10 m, and CLCplus Backbone.

The second tier is represented by vegetation-related products and albedo. CCI Biomass at 100 m reaches a score profile of 3/4 and is therefore relevant for neighborhood-scale interpretation. LAI products are also useful, although in general they remain coarser. Albedo is highly relevant for understanding material-related heat processes, yet the available products are mainly in the 300 m to 1 km range, placing them between district-scale interpretation and broader city context. These variables are therefore more appropriately used as supporting evidence than as the sole basis for local attribution.

Surface radiation budget, precipitation, aerosol properties, and greenhouse gases remain highly relevant from a scientific perspective, but the profiles reported in the inventory indicate that they are substantially better suited to contextual interpretation than to the direct detection of local NBS effects. Surface radiation budget and precipitation products combine very strong record scores with spatial score equal to 1. Aerosol products include one 1 km product, but under the DLR framework this still belongs to the background-context class. Greenhouse gas products are coarser overall, with all listed products remaining in spatial score 1. Their main role is therefore to support inter-city comparison, boundary conditions, and broader explanatory context rather than fine-scale intra-urban assessment.

Product level uncertainty should be considered separately from the limitations associated with local application. First, there is product-specific uncertainty, which is partly documented through the presence of uncertainty layers in the inventory, although not consistently across all products. Several land-cover products do not include an explicit uncertainty layer, and one of the surface-radiation products also lacks this component. Product-level uncertainty is also affected, depending on the variable, by data gaps, retrieval conditions, temporal sampling, and record stability. Infrared LST products, for example, are affected by cloud-related gaps, limited overpass sampling, and additional urban effects related to shading and variable surface emissivity. Albedo products are likewise affected by cloud contamination and variable observation conditions, while BIOMASS CCI requires caution in urban environments because radar/LIDAR-based signals may be influenced by built infrastructure.

A separate issue concerns the limitations of applying these datasets to the objectives of the local study. These limitations arise mainly from the spatial support of the products, the continuity of the available records, and the thematic specificity required for NBS-related interpretation. Even a high-quality product may be of limited use for the local study when its pixel size integrates multiple urban surface types, when their temporal coverage is discontinuous, or when the observed signal reflects a mixture of land cover, urban form, meteorological conditions, and NBS presence, for this reason, the critical assessment presented in Table 3.3 distinguishes between dataset suitability for local application, the main limitations affecting such use, and the proposal mitigation approach.

In addition to scale and attribution issues, product usability for the local study is also constrained by data gaps, temporal sampling, and product stability. Infrared LST products are particularly affected by cloud-related gaps and by limited overpass sampling, meaning that the observed thermal field may not represent the full diurnal behavior of the urban surface. In dense urban areas, shading effects and variable surface emissivity further increase uncertainty. Albedo products are also affected by cloud contamination and variable observation conditions. Moreover, not all products included in the inventory are sufficiently stable for climate-trend analysis, especially when records are short, discontinuous, or affected by changing retrieval conditions. For vegetation-related variables, the use of BIOMASS CCI in urban environments requires caution, as radar/LiDAR-based signals may be influenced by built infrastructure and may therefore be less reliable for direct interpretation within heterogeneous urban areas.

Table 3.3. Critical assessment of the prioritized ECVs using the DLR inventory and local study criteria.

ECV family	Evidence from the DLR inventory	Suitability for the local study	Main limitations for local application	Proposed Mitigation aproach
Land Surface Temperature	CCI LST: 1 km, 31 years, score 1/5; ECOSTRESS: 70 m, 8 years, score 3/3.	Core variable. Strongest direct indicator of urban heat patterns but requires combining coarse long records with finer shorter records.	Scale mismatch between coarse and fine products; cloud-related gaps in IR observations; limited temporal sampling due to fixed overpass times; strong uncertainty in urban areas due to building shading and variable surface emissivity; fine-resolution products often have discontinuous coverage.	Use coarse long-term products as baseline and finer products for recent local analysis; support interpretation with land cover and morphology information; avoid direct trend interpretation from short or discontinuous high-resolution records.

Land Cover	Products from 300 m to 10 m. HRLC 10/30 m reaches 4/5; WorldCover 10 m reaches 4/2; CLCplus reaches 4/3.	Core variable. Best bridge between global and local study because it captures surface heterogeneity and NBS-related classes.	Limited explicit uncertainty information for several products; thematic harmonization across products and cities is needed. classification consistency may vary across time and product families.	Apply a common reclassification across products and cities; use morphology or LCZ classes as the main descriptor for interpreting local thermal differences; cross-check with ancillary greenness/imperviousness information.
Above-ground biomass / vegetation proxies	CCI Biomass: 100 m, 16 years, score 3/4. LAI products: 300 m-1 km, score 2/3 to 1/4.	Useful secondary support for vegetation performance and canopy-related interpretation.	May miss small or recently implemented NBS; proxy meaning differs across products and environments. BIOMASS CCI should be used with caution in urban areas.	Use as supporting vegetation indicators rather than direct NBS-effect measures; interpret BIOMASS CCI with caution in urban areas; cross-check with land cover and greenness information.
Albedo	Products at 300 m-1 km with score profiles from 2/3 to 1/4.	Useful supporting variable for material-related heat processes and district-scale contrasts.	Often too coarse for parcel effects; signal may integrate multiple materials and canopy conditions. Cloud contamination and incomplete temporal coverage can introduce gaps and unstable local sampling.	Use as a supporting variable for district-scale interpretation; interpret jointly with land cover and morphology; avoid using albedo alone for direct attribution of NBS effects.
Surface Radiation Budget	Products at 5.5-25 km with score 1/5.	Contextual variable rather than direct local indicator.	Very coarse support for intra-urban interpretation; one listed product has no explicit uncertainty layer. Useful mainly as contextual forcing rather than direct evidence.	Use only as contextual background information; do not use as a direct indicator of local NBS effects.
Aerosol Properties	CCI Aerosol: 110 km, 1/5; MAIAC Land AOD: 1 km, 1/4.	Contextual variable for air-quality background and city-to-city comparison.	A spatial resolution of 1 km remains too coarse for local NBS analysis. Coverage and retrieval quality may vary with atmospheric and surface conditions.	Use as city-scale or regional atmospheric context; avoid direct attribution of local NBS effects.
Greenhouse Gases	Products from 2.25 km to 500 km, all with spatial score 1 and record scores 3-4.	Contextual variable for emissions framing and broader explanatory analysis.	Very limited intra-urban discriminatory power. Attribution to specific interventions is weak. Records may support regional context but not direct neighborhood-scale attribution.	Use only as broad emissions context and for inter-city comparison; do not interpret as local indicators of NBS effectiveness.

Precipitation	Products at 5.5-10 km with score 1/5.	Contextual hydro-climatic forcing variable; useful for flood and runoff framing.	Insufficient for direct assessment of small urban interventions; needs ancillary local information. Local rainfall variability may not be captured adequately; coarse support limits interpretation of neighborhood-scale hydrological effects.	Use as background hydro-climatic context; support local interpretation with ancillary local information where available.

3.4. Synthesis of dataset suitability and uncertainties

Overall, the assessment supports a two-level strategy. For the global study, the DLR inventory and its original scoring logic provide a robust basis, since long records, broad coverage, and harmonized metadata are essential for comparison across multiple cities. For the local study, the same inventory needs to be interpreted through the morphology–NBS perspective. In practical terms, this implies prioritizing products that provide meaningful local spatial support whenever available, while retaining coarser long-term products as contextual baselines rather than as direct indicators of intra-urban processes.

From this perspective, LST and land cover emerge as the most directly relevant variables for the local study, complemented where appropriate by vegetation-related products and albedo, particularly in relation to canopy, shading, and surface-material effects. Surface radiation budget, aerosols, greenhouse gases, and precipitation remain important within the overall assessment framework, but mainly as contextual variables that support interpretation rather than as variables expected to resolve small-scale NBS effects on their own. High-resolution ancillary layers, particularly imperviousness/greenness information and detailed building descriptors, are therefore essential to reduce scale-related limitations and to support a more robust attribution of local climate signals to urban morphology and NBS.

4. Codesign of the global study

The main objective of the global study is to provide more detailed and comprehensive data and evidence on the relationship between urban morphology and local climate, with the goal to gain new insights into the complex interplay of urban form and the resilience of cities to climate change. To this end,

we systematically combine novel data on the 3D urban structure and urban green spaces with information on local climatic conditions derived from Essential Climate Variables (ECV). In this way, the globally representative study contributes to closing existing information gaps on the potential of EO and ECVs to effectively support local stakeholders in implementing climate services to increase urban climate resilience.

4.1. Selection of cities

The selection of globally representative cities for the global study follows a stratified sampling concept considering the following nine criteria:

- Climate zone (Köppen-Geiger),
- Urban morphotype (according to Taubenböck et al., 2020),
- Topography (e.g., coastal vs. inland; flat/valley vs. plateau/mountain),
- Level of socioeconomic development (Global North vs. Global South),
- Population (including representative number of medium-sized cities),
- Climate threats (for considerable subset of cities),
- Availability of validation data (for subset of cities),
- Consistency with local study cities (see Section 5).

Based on these constraints, a total roster of 159 cities has been defined. This collection includes multiple global megacities per major region (e.g., Tokyo, Shanghai, São Paulo, Delhi, Lagos, Mexico City, etc.) along with explicit blocks of medium cities in Europe, North America, South Asia, Southeast Asia, Africa, and Latin America to capture size-dependent effects. In addition, a representative morphological (e.g., high-rise core, compact block, sprawling suburbia, informal settlements), topographic (coastal ports, inland plains, valleys, plateaus, and mountain cities), and regional (deliberate inclusion of Global South cities and underrepresented African and Latin American medium cities to reduce bias) spread and balance are assured.

Cities with particular climate threats include, amongst others, Dhaka (sea-level/river flooding; extreme rainfall; heat), Jakarta (coastal subsidence; sea-level rise; flooding), Manila (storm surge; pluvial flooding; heat), Ho Chi Minh City (coastal/river flooding; land subsidence), Mumbai and Kolkata (coastal flooding; extreme rainfall; heat), Lagos (coastal flooding; informal settlement exposure), Shanghai and Guangzhou (coastal flooding; storm surge; heat), New York and Miami (sea-level rise; storm surge; heat), Mexico City, Quito and La Paz (air stagnation; heat; water stress), Bangkok (river/coastal flooding; subsidence), Cairo (coastal flooding; water stress), and Phoenix, Delhi and Karachi (extreme heat and heatwave exposure).

The complete list of cities along with their key characteristics is provided in Table A.1 in Annex I.

4.2. Data sets for the global study

The implementation of the global study considers the collection and preparation of data for four thematic blocks, namely i) the delineation of the city areas, ii) the characterization of 3D urban morphology, iii) the description of urban green and imperviousness, and iv) the characterization of the local climate.

It must be noted that the same data sets will be also used for the local studies, although the spatial scale to which they will be considered is going to be different, as highlighted in Section 5.

4.2.1. Delineation of the city areas

For the spatial delineation of the city footprints for the selected metropolises, we use the Global Human Settlement (GHS) Urban Centre Database (UCDB) in the release version 2024 (GHS-UCDB R2024A), provided by the European Commission's Joint Research Centre (JRC). The GHS-UCDB R2024A is a harmonized, multi-temporal global inventory of urban centers explicitly designed to support comparative urban science, policy monitoring and large-scale data-driven modelling (Melchiori et al., 2024). The product builds on the Global Human Settlement Layer (GHSL) family of raster and vector layers (e.g., built-up area, population grids, degree of urbanization) to deliver a quality-controlled set of 11k+ urban center polygons together with a broad suite of aggregated indicators spanning built environment, population, land cover, accessibility, exposure and selected risk and emissions proxies. GHS-UCDB R2024A emphasizes reproducibility and metadata transparency: each urban center is accompanied by provenance metadata, quality flags and epochal attributes that enable change-over-time analyses (derived from GHSL epochs and ancillary open datasets). Methodologically, the UCDB delineation follows a standardized workflow that first identifies urban extents using the degree-of-urbanization approach (Schiavina, Melchiorri and Pesaresi, 2023) and GHSL built-up layers (Florczyk et al., 2019), then aggregates raster-based metrics (e.g., built-up fraction, population density, land-cover fractions) and links administrative and socioeconomic contextual variables to each urban center polygon. This approach yields a dataset that is directly comparable across countries and time steps, making it particularly well suited as a sampling frame for global comparative studies, for training and validating machine-learning models, and for stratified analyses of urban form–impact relationships.

However, many of the UCDB indicators are derived at nominal resolutions of ~1 km or coarser and therefore do not capture parcel- or building-scale 3D morphology (e.g., mean building height, façade orientation, street canyon geometry). Moreover, the temporal coverage and indicator completeness vary by region and epoch, and some proxies (e.g., built-up fraction as a surrogate for imperviousness) carry systematic uncertainties that should be quantified in any inference. The dataset is openly distributed through the JRC/GHSL data catalogue (JRC, 2026).

As part of the tailoring process of the dataset to the needs of the MOMO-NBS project (see D2.2_MOMO-NBS_TailoredDataDeliveryNote_v1.0 for more details), the GHS-UCDB R2024A polygons for the selected cities are extracted and then supplemented by an additional, buffered version (50 km buffer distance) in order to be able to consider the surroundings of the cities in the intended MOMO-NBS analyses of the global study.

4.2.2. 3D urban morphology

To characterize the 3D urban morphology, we use DLR's novel World Settlement Footprint 4D (WSF® 4D) data (Esch et al., 2026). The WSF® 4D combines existing state-of-the-art building footprint (BF) datasets and assigns information on area, height, volume, and year of construction to each single building (see Fig. 4.1). The resulting building model (level of detail 1 – LoD 1) comprises a total of 2.7 billion footprints worldwide and represents the most complete, up-to-date, and accurate instance-level building footprint BF layer available to date. At the same time, it is the first source of information to describe the global, spatiotemporal growth pattern of building stock over the last four decades. Therewith, the WSF® 4D provides an ideal dataset to support a systematic investigation of the relationship between urban morphology and local climate.

The highly automated, modular processing framework implemented to generate the global WSF® 4D dataset consists of three main processing blocks: i) the generation of a building footprint layer, ii) the assignment of a building height and volume to each building polygon, and iii) the estimation of the year of construction (only for newly developed areas outside the previously existing settlement area and not for reconstructed buildings within the built-up area).

The basic principle for creating the WSF® 4D building footprint layer (processing block i) follows the approach of starting from a curated building footprint dataset with a correspondingly high quality which is then – building by building – sequentially compared to and supplemented by additional building footprint datasets. As an initial data source for generating the global WSF® 4D building

footprint layer, the constantly updated and curated building database provided by the Overture Maps Foundation is used (Overture Maps Foundation, 2026). This free and open collection holds information on six data themes (addresses, buildings, base, divisions, places, and transportation). The Overture Maps Foundation's building footprint dataset (OMF-B) is a combination of various open building layers that are used with different conflation priorities, namely Open Street Map (OSM), Esri Community Maps, Instituto Geográfico Nacional, City of Vancouver, Google Open Buildings, and Microsoft's GlobalMLBuildingFootprints. In addition, the WSF® 4D layer integrates BF of the OpenBuildingMap (OBM) introduced by Oostwegel et al. (2025) as well as building outlines extracted via an image segmentation approach from the Google Open Buildings 2.5D Temporal (GOB2.5D) dataset (Sirko et al., 2023). Finally, 3D Global Building Footprints (3D-GloBFP) layer is considered for the area of China. (Che et al., 2024).

Using the previously generated WSF® 4D building footprint layer, a second processing module (processing block ii) assigns a height value to each individual building polygon (see Fig. 4.1b). The assignment is again conducted sequentially, according to the following order – or priority – of the height data sources: First, the OMF-B data is again considered (Overture Maps Foundation, 2026). OMF-B also offers information on building heights for specific regions (e.g., USA or Europe). Next, the GOB2.5D raster dataset derived for the year 2023 and covering the countries of the Global South (~58 million km^2) is employed (Sirko et al., 2023). The GOB2.5D estimates the building height based on open Sentinel-2 satellite imagery using an AI-model. Other, globally available input source of height data are the WSF® 3D (Esch et al., 2022) - a layer providing information on the total area, average height, and total volume of buildings at 90m resolution – and the GHSL Building Height (Pesaresi et al., 2024), referencing the year 2023 (GHS-BUILT-H R2023) and giving information on the average of the net building height at a gridding of 100m. Finally, for Asia, the 3D-GloBFP is considered again (Che et al., 2024).

Despite the availability of global settlement layers and large-scale databases of building footprints, the building footprint datasets are not updated at regular intervals, making them quickly outdated in fast-growing regions, particularly in Africa and Asia. To bridge this gap, DLR has developed the novel World Settlement Footprint tracker (WSF® tracker) dataset. The WSF® tracker provides the first consistent monitoring of global settlement extent at 10m resolution, updated every six months from July 2016 to the present. The WSF® tracker is based on an enhanced version of the methodology used to generate the WSF® 2019 (Marconcini et al., 2021). This approach analyses multitemporal collections of multispectral Sentinel-2 (S2) and radar-based Sentinel-1 (S1) satellite imagery in

order to depict the distinct temporal behavior of human settlements in radar backscatter and spectral signature, which differ significantly from those of non-settlement classes. The process begins by collecting images over a region within a set period with minimal expected changes, from which temporal statistics of key radar and optical features are extracted (e.g., median of vegetation/built-up/water index or polarimetric decomposition indices over an interval of one year). Training samples for settlement and non-settlement classes are generated using thresholds that vary based on Köppen-Geiger climate zones and – as reference – the built-up area defined by the merger WSF® 2019 and building footprint layers rasterized to 10m-resolution (e.g., MS-GMLBF, GOB, and OSM). Finally, a Random Forest binary classification is applied and information from suitable ancillary datasets is considered to further reduce omission and commission errors (e.g., information on slope derived from digital elevation model data and information on the road network provided by Open Street Map). The workflow has been employed on the Google Earth Engine platform to derive 10m resolution binary settlement masks at 6-months-intervals from 2016 to 2025, finally resulting in 19 classification maps (as of July 2025).

Due to the fact that the Sentinel satellite data – on which the WSF® tracker is based – has only been available since 2016, we use alternative data to determine the year of construction for settlement areas developed before 2016. For this purpose, the World Settlement Footprint evolution (WSF® evolution) is employed (Marconcini et al., 2021). The WSF® evolution is derived from Landsat-5/7 satellite images and represents a 30 m resolution dataset outlining the global settlement extent on a yearly basis from 1985 to 2015. The WSF® evolution methodology corresponds to that previously described for the WSF® tracker, with the difference that, in addition to the analysis of Landsat data, the 30 m WSF® 2015 (Marconcini et al., 2020) settlement mask (also derived from Landsat) formed the reference basis, instead of the higher resolution WSF® 2019 settlement mask (which was not yet available at the time of the WSF® evolution production). Here it is worth noting that the availability of Landsat data considerably varies across the world and over time. Independently from the implemented approach, this can result in a lower quality of the generated settlement masks in regions where only few or even no Landsat scenes have been collected. Accordingly, to provide the users with a measure accounting for the coverage of the Landsat imagery, the WSF® evolution conceives the Input Data Consistency (IDC) score, which ranges from 6 to 1 with: 6) very good; 5) good; 4) fair; 3) moderate; 2) low; 1) very low.

The year of construction of the individual buildings is estimated to be using the WSF® tracker and WSF® evolution datasets. For this purpose, the WSF® 4D building polygons and the WSF® tracker are spatially intersected, whereby for

each WSF® 4D building the dominating year of construction is determined by a zonal statistics calculation (majority function) based on the WSF® tracker raster dataset. For all buildings that already existed in 2016 according to the WSF® tracker, the year in which the building – or the built-up neighborhood – appeared, is indicated by a corresponding attribute. For all remaining building footprints without an indication of the construction year, the WSF® evolution – describing the settlement extent between 1985-2015 on an annual basis – is analyzed to define the year of construction. Figure 4.1c shows a per-building visualization of the estimated year of construction.

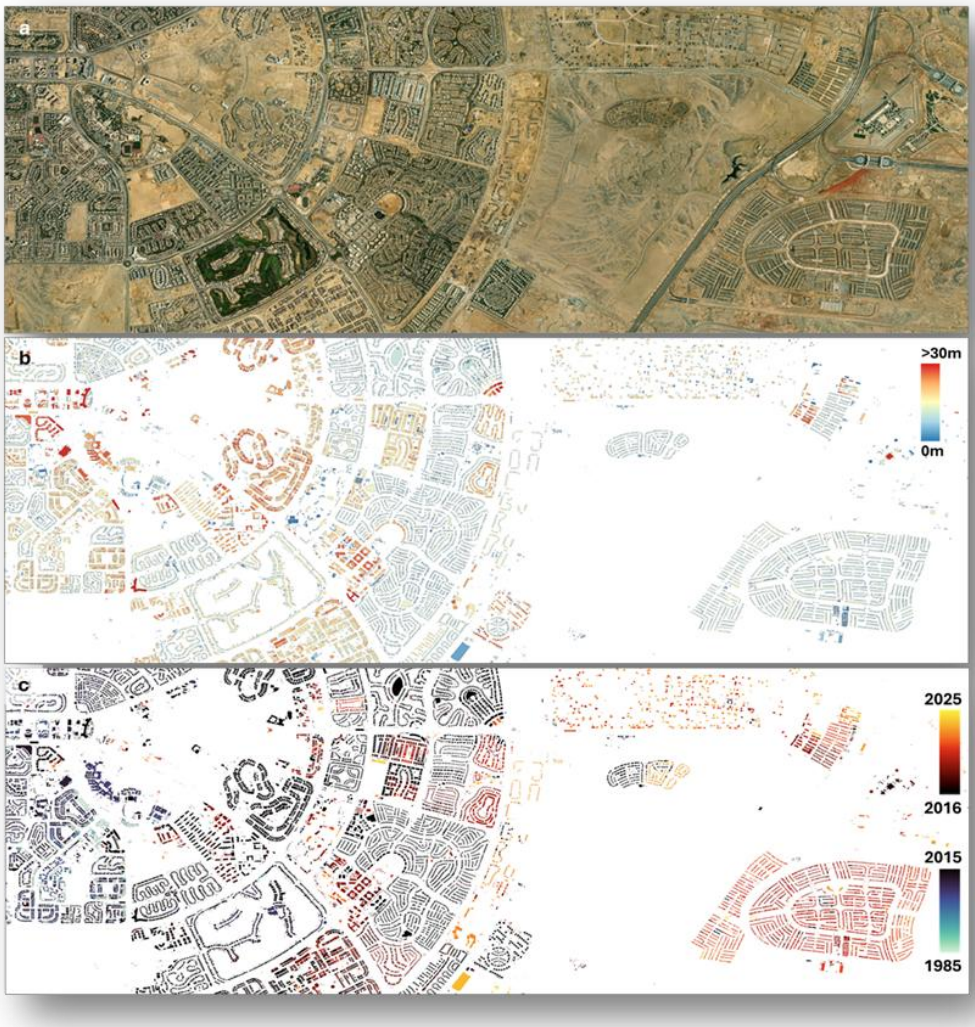

Fig. 4.1: Building pattern in the area of New Cairo, Egypt (a) and building height (b) and estimated year of construction (c) provided by the novel WSF® 4D dataset.

4.2.3. Climate-relevant city structuring

To describe the climate-relevant city structuring, we have implemented an approach to map the urban greenness and imperviousness. For this purpose, multitemporal collections of multispectral Sentinel-2 satellite imagery are analyzed to depict the distinct spectral signature and temporal behavior of vegetation-covered and impervious surfaces within the settlement area. The process begins with collecting images over a region of interest, for which - after cloud-masking of each single input image - temporal statistics (e.g., mean, minimum, maximum, percentiles over the given period – e.g., 12 months) of the Normalized Difference Vegetation Index (NDVI) are extracted for a flexibly definable period. A period of 12 months is used for the processing of urban greenness and imperviousness in MOMO-NBS. Finally, a Machine Learning approach (e.g., Support Vector Regression) is trained and applied to estimate the percent green area – or, as inverse, the impervious surface – within each 10m pixel of the input Sentinel-2 NDVI temporal statistics data (see Fig. 4.2a). The resulting dataset $GreenImp_{EO}$ shows a value range of 0-100, with a value of 100 representing areas with 100% vegetation cover (or, in a simplified assumption of the urban surface, 0% imperviousness), whereas a value of 0 represents regions with no vegetation and 100% imperviousness. Here it is important to note that the analysis is exclusively focused on the settlement area using the GHS-UCDB R2024A urban cluster polygons.

In a subsequent step, the modelled raw greenness/imperviousness dataset is enhanced based on the integration of road data from OpenStreetMap (OSM) and building footprints provided by the WSF® 4D. OpenStreetMap (OSM) is a volunteer-contributed, wiki-style geospatial database whose core strengths are global coverage, rapid update frequency, rich semantic tagging and an active ecosystem of tools and derivatives. Contributors map features at varying scales, and the project publishes full database dumps (the “planet” file) and regional extracts for research and operational use.

The optimization procedure starts with the calculation of the total road and building area within each single 10m-pixel of the initially modelled greenness/imperviousness layer. Here, the area of road surface is derived from the total length and width of OSM road segments within each given pixel, whereas the building area is defined by the summarized area of WSF® 4D building footprints within this 10x10m raster cell. Next, the sum of the road and building area is divided by the total pixel area (10x10m = 100m^2) in order to define the percent impervious surface for each pixel. As a value of 0 corresponds to an imperviousness of 100% in the EO-modelled greenness/imperviousness layer $GreenImp_{EO}$, the imperviousness fraction derived from WSF® 4D has to be

subtracted from the value 1 in order to ensure a scaling which is identical. Finally, the resulting greenness/imperviousness value $GreenImp_{OSM/WSF}$ is compared to the greenness/imperviousness value of $GreenImp_{EO}$ (shown in Figure 4.2a) by means of a Minimum function:

$$GreenImp_{final} = MIN\,[GreenImp_{EO}\,,\, GreenImp_{OSM/WSF}] \qquad Eq.\ 4.1$$

Considering Equation 4.1, the initial $GreenImp_{EO}$ is replaced if $GreenImp_{OSM/WSF}$ shows a lower value – meaning a higher imperviousness (or lower greenness). This approach can effectively improve underestimated sealed areas – for example, when sealed areas such as streets and squares are overhung by tree crowns or building roofs are greened.

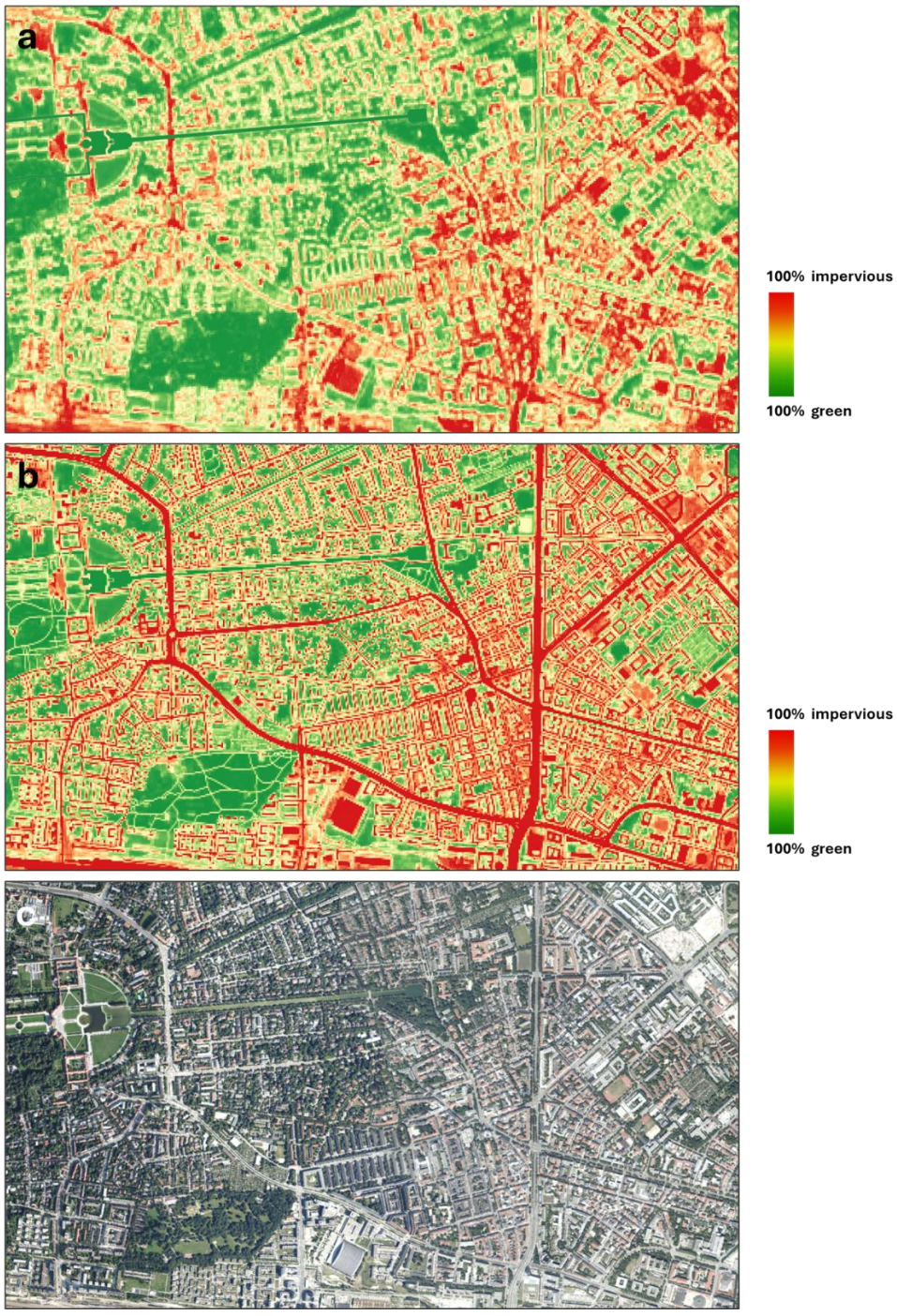

Fig. 4.2: Initial version of the 10m greenness/imperviousness layer modelled from multi-seasonal Sentinel-2 imagery (a), final version enhanced by refinement with road data from Open Street Map and building footprints provided by the WSF®4D (b), and – for comparison purposes – very high-resolution image of the same region.

In addition, we use Local Climate Zone (LCZ) data, which is described in more detail in section 5.2.1.

4.2.4. Urban climate

To characterize the climate conditions of the selected cities, a set of Essential Climate Variables (ECVs) is compiled from ESA Climate Change Initiative, Copernicus Climate Data Store (CDS) and complementary sources. For each of the 159 selected cities, zonal statistics of the ECV datasets are calculated across two spatial configurations: the GHS-UCDB R2024A urban centre polygon itself, capturing the intra-urban climate signal, and a surrounding 50 km buffer zone, capturing the larger regional climate context within which each city is located.

The primary thermal variable is Land Surface Temperature (LST), sourced from the CDS multi-instrument record spanning June 1995 to the present at 0.01° × 0.01° (~1 km) monthly resolution, produced from inter-calibrated ATSR-2, AATSR, Terra MODIS, and Sentinel-3B SLSTR observations. Separate daytime and nighttime LST layers are retained to distinguish the distinct physical regimes of solar-driven daytime heating and nocturnal heat release. The Surface Urban Heat Island (SUHI) intensity is subsequently derived from the zonal statistics computed for the urban polygon and its surrounding buffer, respectively. Surface albedo is sourced from the CDS 10-daily gridded dataset available from 1981 to the present, with the broadband directional (black-sky) albedo used as the primary variable, spatial resolution varies by sensor generation, from approximately 4 km (AVHRR, 1981–2005) to 1 km (SPOT-VGT/PROBA-V, 1998–2020) to 300 m (Sentinel-3, 2018–present). The Surface Radiation Budget (SRB), quantifying the balance between surface heating via solar absorption and cooling through infrared emission across incoming, outgoing, and net radiation flux components, is sourced from two product families spanning 1979 to the present: the ESA/C3S Cloud_cci record at 0.5° spatial resolution and the EUMETSAT CM SAF CLARA-A3 record at 0.25° spatial resolution with daily shortwave means.

Near-surface air temperature and precipitation are sourced from the CDS ERA5-Land monthly averaged reanalysis at ~9 km spatial resolution and included as further local climate descriptors, as background thermal forcing and rainfall seasonality are relevant contextual variables when assessing urban climate conditions across the climatically diverse global city sample. Additionally, wind speed and direction are also derived from ERA5-Land as the 10 m U and V wind components.

Aerosol optical depth (AOD), sourced from the ESA-CCI merged sensor record at 1° × 1° spatial resolution and monthly temporal resolution, is included as an ECV descriptor of the atmospheric environment of each city. Atmospheric greenhouse gas concentrations, that is specifically column-averaged CO_2 (XCO_2) and CH_4 (XCH_4) from the respective CDS multi-sensor merged Level 3 products at 5° × 5°

spatial resolution and monthly temporal resolution spanning October 2002 to the present. Given their coarse spatial resolution, AOD and the greenhouse gas concentration records are treated as city-region characterizers rather than intra-urban variables.

Land cover is sourced from the ESA-CCI annual global map at 300 m spatial resolution, and above-ground biomass (AGB), sourced from the ESA-CCI merged product at 100 m spatial resolution and annual temporal resolution, are included as ECV-based descriptors of the surface composition and vegetation carbon stock of each city and its surroundings. Soil moisture is sourced from the ESA-CCI passive microwave merged product at ~25 km spatial resolution and daily temporal resolution and is included as an additional surface state variable.

Together, the local climate variables derived from the ECVs described above are combined with the urban form variables, imperviousness fraction, greenness fraction, 3D building structure, and street network characteristics, to assess statistical relationships between urban morphology and climate outcomes across the global city sample.

The two-configuration design, that is the GHS-UCDB urban-center polygon and its surrounding 50 km buffer, follows the cross-city indicator framework set out in the Science Requirements Document (SRD) (Section 6.2), which calls for a common reporting unit enabling cross-city comparison (science-driven requirement) together with at least one intra-urban stratification scheme (stakeholder-driven requirement). The former is provided by the urban-polygon/buffer pairing, while the latter is realized through the concentric-ring subdivision described in Section 4.3.3. The specific zonal statistics computed for each configuration (e.g., mean, median, and selected percentiles, etc.) will be refined during the analysis and are detailed alongside the statistical treatment in Section 4.3.4. Because the long ECV records carry known limitations, including sensor-generation discontinuities, resolution changes across instrument eras, and gap or stability issues (some of which are noted above for albedo, LST, and the surface radiation budget), the analysis will favor relative measures between zones over absolute values where appropriate. The SUHI intensity, derived as the urban-minus-buffer difference, is the primary example: differencing co-located zones cancels much of the shared absolute bias and instability inherited from the underlying records. This is consistent with the SRD requirements for attribution and confounding control and for uncertainty characterization. Further measures such as seasonal baselining, anomaly-based comparison, or restriction to homogeneous sub-periods will be considered depending on the data behavior

observed during the analysis. The following figure summarizes the described method as a workflow diagram.

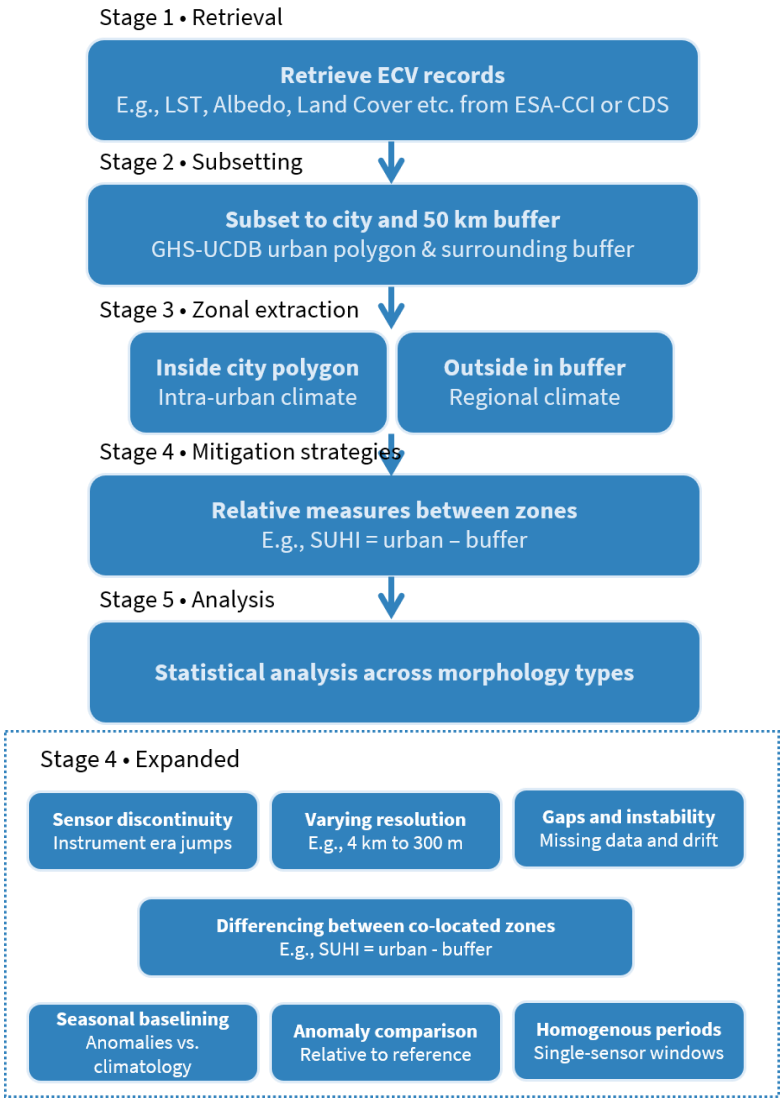

Fig 4.3: Workflow concept for the ECV-based urban characterization, For each of the 159 cities, the GHS-UCDB urban-center polygon (inner shape) is nested within a surrounding 50 km buffer (outer ring); zonal statistics are computed separately for each zone, and their difference (urban − buffer) isolates the intra-urban climate signal from the regional context while cancelling much of the bias and instability shared by the underlying records, as exemplified by the SUHI intensity. The same two zones are applied consistently across all co-registered ECV layers (e.g., LST, albedo, surface radiation budget, ERA5-Land variables, AOD, greenhouse gases, land cover, above-ground biomass, and soil moisture), yielding per-zone metrics for every variable. Stage 4 – Expanded shows the measures taken against ECV limitations if differencing between co-located zones proves insufficient.

4.3. Methodology

4.3.1. Analytical framework

This study investigates associations between urban morphology and urban climate across a globally representative sample of cities. Specifically, it aims to identify patterns linking urban form, three-dimensional built structure, green and blue infrastructure, and street-network characteristics with EO-derived climate variables. By integrating detailed urban morphological information with Essential Climate Variables (ECVs), the analysis provides a consistent framework for assessing how urban structure relates to local climatic conditions and, ultimately, to urban climate resilience.

The analysis includes 159 representative cities worldwide, as defined in Annex 1. The selection criteria are described in Chapter 4.1. Two spatial configurations are considered: (i) the full urban extent including a surrounding buffer area, and (ii) the intra-urban structure. City boundaries are delineated using the Global Human Settlement Urban Centre Database, release 2024 (GHS UCDB R2024A), as described in Chapter 4.2.1.

Urban morphology is characterized by using indicators of impervious surface fraction, green and blue infrastructure, three-dimensional building morphology, and street-network structure. These variables are analyzed in relation to EO-based climate indicators, including Land Surface Temperature, Land Cover, vegetation proxies, albedo, Surface Radiation Budget, aerosol properties, greenhouse gases, and precipitation.
All datasets are collected, re-gridded, and oversampled to a common spatial resolution of 10 m × 10 m, following previous work (Müller et al., 2023; Iungman et al., 2024; Erbertseder et al., 2024). This harmonized grid forms the basis for all subsequent analyses.

4.3.2. Identification of urban morphology types

To identify distinct urban morphology types and assess their relationship with urban climate, we apply Uniform Manifold Approximation and Projection (UMAP) (McInnes et al., 2018), followed by k-means clustering (Lloyd, 1982). UMAP is a non-linear dimensionality reduction technique that preserves the manifold structure of high-dimensional datasets in a low-dimensional embedding. It was selected because of its computational efficiency and its ability to preserve global data structure better than earlier approaches such as t-SNE.
Each city is represented in the UMAP analysis using the full set of variables described in Chapter 4.2. The resulting low-dimensional embedding is evaluated

in relation to the distribution of the input variables and subsequently used as input for k-means clustering. The optimal number of clusters is determined using the Elbow method (Thorndike, 1953).

4.3.3. Intra-urban analysis

To assess intra-urban variability in a harmonized way across all cities, each city is subdivided into five concentric rings following the Burgess model (Burgess, 1925). Urban center coordinates are extracted from the OSM Nominatim database (OpenStreetMap Collaborators, 2015), and the distance from the city center to the centroid of each grid cell is calculated. Grid cells are then assigned to one of five rings based on the quintile distribution of these distances. For each ring within each city, mean values are calculated for all variables and used in the subsequent analyses.

To further characterize the influence of urban morphology on urban climate, we incorporate Local Climate Zone (LCZ) (Stewart and Oke, 2012) and OpenStreetMap (OSM) (OpenStreetMap, 2026) variables for each city and for each of the five concentric rings as supplementary inputs to the UMAP analysis. Only cities with complete datasets are included. The optimal number of clusters is again determined using the Elbow method. The LCZ classification provides a universal and standardized description of urban form. Based on satellite imagery, the LCZ framework classifies urban landscapes according to building density and height, imperviousness, and vegetation characteristics into 17 classes: 10 built types (compact high-rise, compact mid-rise, compact low-rise, open high-rise, open mid-rise, open low-rise, lightweight low-rise, large low-rise, sparsely built, and heavy industry) and 7 natural land-cover types (dense trees, scattered trees, bush or scrub, low plants, bare rock or paved surfaces, bare soil or sand, and water) (Stewart and Oke, 2012). For this study, we use the LCZ classification developed by Demuzere et al. (2020). We overlay the LCZ layer with the analysis grid and estimate, for each grid cell, the proportion of area corresponding to each LCZ class.

To characterize street-network design, we derive the density of distinct road typologies from the OSM database. The following road classes are considered: motorized roads (motorway and trunk), primary roads, secondary roads, tertiary roads, residential roads (unclassified, residential, and living streets), pedestrian zones, and cycleways. For each grid cell, we calculate the total length, in meters, of each road type.

4.3.4. Statistical analysis

Statistical differences of all 159 cities are assessed for both (i) the full city extent and (ii) the five intra-urban rings across the identified urban morphology types and tested regarding significance. The variables evaluated include Land Surface Temperature, Land Cover, vegetation proxies, albedo, Surface Radiation Budget, aerosol properties, greenhouse gases, and precipitation. Depending on the spatial resolution of the ECV datasets, the ring-based approach may not be applicable to all variables; this will be evaluated during the course of the project.

Because not all variables are expected to satisfy assumptions of normality and homogeneity of variance, non-parametric tests are applied where appropriate. Specifically, we use the Kruskal-Wallis test followed by Dunn's post hoc test (Iungman et al., 2024; Erbertseder et al., 2015). Given the expected variability in both urban morphology and urban climate across concentric rings, analyses are conducted separately for each ring. For some ECV datasets, the ring-based approach may not be applicable due to spatial resolution constraints; this will be evaluated during the analysis.

5. Codesign of the local study

The local study aims at design, together with the local stakeholders a city-level NBS monitoring, i.e., a study about NBS monitoring at the intra-city scale by combining ECVs with more spatially and temporally detailed 2D/3D morphological information extracted from EO data sets. This study will assess the feasibility of capturing the effectiveness of climate change resilience projects using currently available Essential Climate Variables (ECVs). Additionally, it will provide recommendations on the necessary improvements in the spatial resolution of existing ECVs to enable accurate monitoring of the effects of Nature-Based Solutions (NBS) on the urban climate.

5.1. Selection of the cities for the local study

The selection of the case study cities defines the spatial framework within which the relationship between urban morphology. Essential Climate Variables (ECVs). and the effectiveness of Nature-Based Solutions (NBS) will be analyzed. The objective of this selection process was to identify a set of cities that are both diverse and comparable. enabling the project to test the proposed analytical framework across different climatic. morphological and governance contexts while maintaining methodological consistency.

To achieve this objective. The selection of the ten cities followed a structured approach based on four main criteria:

1. Engagement of stakeholders;
2. Presence or absence of NBS;
3. Representation of different climate zones;
4. Comparable urban scale and morphology diversity.

These criteria ensure that the selected cities provide a balanced sample capable of supporting both the global-scale analysis of urban climate dynamics and the city-level monitoring of NBS effects envisaged in the project. The resulting set of cities includes Cairo, Hamburg, Beijing, Kigali, Singapore, Madrid, Milan, Córdoba, Stockholm, and Calgary, representing different geographical regions and urban development patterns.

The first fundamental criterion for the selection of the cities was the presence of engaged stakeholders, including municipalities, national agencies, and research institutions connected to the project consortium or previously involved in collaborative initiatives.

Several of the selected cities are directly linked to the project partners or associated stakeholders. Their inclusion ensures the availability of local knowledge, planning documents, and datasets which are essential for validating the presence or not of NBS.

These cities also represent important examples of European metropolitan areas that have actively implemented climate adaptation policies and urban greening strategies in recent years. Their participation allows the project to test the proposed methodology in contexts where NBS interventions are already integrated into urban planning processes, providing valuable case studies for understanding how urban morphology interacts with climate adaptation measures.

In addition to these European examples, the selection includes cities from other global regions such as Cairo, Beijing, Singapore, Kigali, Córdoba, and Calgary. The inclusion of cities from different institutional and governance contexts is essential for evaluating the applicability of the project methodology beyond Europe. In particular, cities such as Córdoba represent rapidly developing urban environments where climate adaptation strategies are still evolving, offering the opportunity to analyze how morphological and environmental indicators behave in contexts where NBS implementation is emerging or limited.

The presence of stakeholders and institutional connections therefore plays a dual role in the project. On the one hand, it facilitates the co-design approach adopted in MOMO-NBS, allowing local actors to contribute to the interpretation of results and to the identification of relevant NBS initiatives. On the other hand, it ensures that the selected cities provide realistic and policy-relevant case studies, strengthening the potential impact of the project's outcomes.

A second key criterion in the selection process was the presence or absence of Nature-Based Solutions within the urban environment. The objective of the project is not only to analyze cities where NBS are already widely implemented, but also to compare these contexts with cities where such strategies are still limited or emerging.

Cities such as Singapore, Hamburg, Madrid, and Milan are internationally recognized examples of urban environments where NBS have been systematically integrated into planning policies and climate adaptation strategies.

In contrast, cities such as Córdoba or Cairo represent contexts where NBS strategies are less consolidated or still under development. Their inclusion is important because it allows the project to analyze the potential effectiveness of NBS under different stages of implementation and planning maturity. Comparing cities with extensive NBS policies to those where such measures are limited provides an opportunity to better understand how urban morphology influences the capacity of cities to integrate nature-based climate adaptation strategies.

Another fundamental criterion in the selection process was the representation of different climate zones, as reported in the project dataset. Climate conditions play a central role in shaping urban climate dynamics and determining the effectiveness of NBS interventions. For this reason, the selected cities were chosen to represent a wide range of climatic contexts.

The sample includes cities located in different climate zones based on the Köppen–Geiger climate classification: humid continental, temperate oceanic, tropical savanna, tropical rainforest, Mediterranean, humid subtropical. For the city of Calgary, which is included in humid continental, cold semi-arid area, climate challenges are often related to seasonal temperature variability and snow-related processes. This city provides an important case study for analyzing how urban morphology interacts with climate variables such as land surface temperature, soil moisture, and atmospheric conditions in northern environments.

Other cities represent humid subtropical climates, including Milan. These environments are characterized by increasing heat stress, drought conditions, and urban heat island effects, making them particularly relevant for studying the cooling potential of urban vegetation and blue-green infrastructure.

Cities such as Kigali and Singapore represent tropical climates (tropical savanna and rainforest), where strong seasonal variations and urban pollution dynamics interact with the built environment. In these contexts, urban morphology can significantly influence wind patterns. air circulation and pollutant dispersion.

By including cities from different climate zones, the project aims at evaluating whether the relationships between urban morphology, ECV indicators, and NBS effectiveness remain consistent across climatic conditions or whether they vary significantly depending on environmental context.

While ensuring climatic and geographical diversity, the selection process also aimed to maintain a comparable urban scale among the selected cities. This aspect is particularly important for the analysis of satellite-derived indicators. as differences in spatial scale can significantly affect the interpretation of morphological metrics such as built-up density, green fraction or water coverage.

Although the selected cities are in different parts of the world, they share broadly comparable urban extents and metropolitan dimensions, making them suitable for comparative analysis. This allows the project to evaluate morphological indicators derived from Earth Observation datasets under similar spatial conditions, reducing biases related to extreme differences in city size.

At the same time, the selected cities exhibit a high degree of morphological diversity, which is essential for testing the central hypothesis of the project. European cities such as Milan and Madrid are characterized by relatively compact urban fabrics with historical centers and dense residential districts. Northern European cities such as Stockholm and Hamburg include significant waterfront areas, and extensive green networks integrated into the urban structure.

In contrast, cities such as Calgary display more dispersed urban patterns typical of North American urban development, while Beijing represents a large metropolitan system characterized by high-density development and rapid urban expansion. Singapore offers an example of a highly dense tropical city where urban vegetation and water management play a central role in shaping the urban environment.

This diversity of urban forms enables the project to investigate how different morphological configurations influence urban climate dynamics and the

effectiveness of NBS interventions. By analyzing cities that differ in density. structure and spatial organization, the project can better understand the interactions between built environments. vegetation and climate variables.

The final selection of the ten case study cities therefore reflects a deliberate balance between diversity and comparability. By combining cities with different climatic conditions, levels of NBS implementation and urban morphologies, the project wants to create a framework for testing the relationship between urban forms, ECVs, and NBS.

COUNTRY	CITY	MORPHOLOGY	INHABITANTS	CLIMATE ZONE	CITY AREA km²	GREEN AREA %
Egypt	Cairo	compact low-rise, compact mid-rise, open low-rise	10.100.000	Hot-desert	1.604,55	26.16%
Germany	Hamburg	open mid-rise+compact high-rise+open high-rise+large low-rise+heavy industry	1.946.000	Temperate-oceanic	747.47	69.97%
China	Beijing	open mid-rise+open high-rise+compact high-rise+compact mid-rise	19.340.000	Humid-continental	2.264.09	47.41%
Rwanda	Kigali	compact low-rise+open low-rise	1.746.000	Tropical-savanna	737.46	78.04%
Singapore	Singapore	compact high-rise+open high-rise+open low-rise+large low-rise+compact low-rise	5.918.000	Tropical-rainforest	1.716.47	22.76%
Spain	Madrid	compact mid-rise, open mid-rise, open low rise	3.300.000	mediterranean	8.021.70	67.68%
Italy	Milan	compact mid-rise	1.362.000	Humid-subtropical	181.79	38.61%
Argentina	Cordoba	compact low-rise+open low-rise+large low-rise+compact mid-rise	1.505.000	Tropical-rainforest	575.51	59.98%
Sweden	Stockholm	compact high-rise+compact mid-rise+open high-rise+large low-rise	988.000	Humid-continental	215.78	55.93%
Canada	Calgary	compact high-rise+open mid-rise+open low-rise+large low-rise	1.414.000	Humid-continental	849.25	59.42%

5.2. Data sets used for the local studies

In addition to the data set already mentioned in Section 4.2, which for the local studies will be considered at the finest spatial resolution, two additional data sets will be considered.

5.2.1. Local Climate Zone maps

The Local Climate Zone (LCZ) classification was used to characterize the intra-urban morphological structure of the selected cities, providing a standardized framework to relate urban form to the climate and environmental conditions.

The LCZ scheme defines a set of standardized urban and natural classes based on surface cover, structure, materials, and anthropogenic activity. In particular, it distinguishes between:

- built-up classes, representing different urban morphologies (e.g. compact high-rise, open mid-rise, large low-rise),
- and land cover classes, representing natural surfaces such as vegetation, bare soil, or water.

LCZ maps were generated using satellite-based Earth Observation data processed within the Google Earth Engine environment, enabling large-scale and consistent classification across cities.

The relevance of the LCZ-based approach is further supported by the diversity of urban morphologies observed across the selected case study cities, as summarized in the table.

The cities exhibit a wide range of morphological configurations, including:

- compact urban fabrics (e.g., Milan, Madrid), characterized by dense mid-rise structures;
- high-density metropolitan systems (e.g., Beijing, Singapore), including compact and open high-rise typologies;
- mixed and heterogeneous morphologies (e.g., Hamburg, Stockholm), combining open mid-rise, industrial areas, and extensive green networks;
- and low-rise or rapidly developing urban forms (e.g., Kigali, Cordoba), where open and large low-rise structures dominate.

This diversity is also reflected in the proportion of green areas, which ranges from approximately 22% in Singapore to nearly 70% in Hamburg, highlighting significant differences in the presence of vegetation and potential NBS.

Such variability ensures that the LCZ classification captures a broad spectrum of urban forms, enabling the analysis across different environmental and geographical contexts.

5.2.2. Nature-based solution historical information and maps

To complement the morphological characterization, information on NBS was collected for the selected cities. NBS data were derived from a combination of international databases and local sources, including:

- NATURVATION;
- OPPLA;
- official municipal websites and planning documents of the case study cities;
- direct contact with stakeholders.

The collected NBS information was processed through the following steps:

1. Data collection and screening: identification of relevant projects related to urban greening, blue-green infrastructure, and ecosystem-based adaptation measures.
2. Temporal attribution: each NBS was associated, when possible, with an implementation period or reference year
3. Classification and harmonization: NBS were categorized into classes (e.g. urban parks, green corridors, water-based solutions, green roofs), ensuring comparability across cities.

Despite these efforts, some limitations remain, particularly related to:

- incomplete spatial coverage,
- variability in data quality across cities, and
- lack of replies from some of the stakeholders.

The results of this analysis are summarized in the following table, where the information about all the NBS projects that have been found so far for the ten test cities has been summarized. The project team will keep working to improve the current set of information, refining the coarser attributes that have been obtained so far and adding new NBS and their features to the current list.

Table 5.1: the selected 10 urban areas used for the local study.

City	What	Planned	Realized	Where	How much	When	Web sources
Cairo	/			/	/		
Hamburg	The cleaver way : green corridor, green roofs and facades, schoolyards		x	Neugraben-Fischbeck	220.76ha		https://oppla.eu/clever-cities/case-study/clever-way-
	Wilhelmsburg Island: park		x	Inselpark	9ha		https://una.city/nbs/hamburg/island-park-wilhelmsburg-
	Covering the A7 highway: green roofs, parks and urban forests, community gardens	x		south-north highway (A7)	250.000mq	2012-2028	https://una.city/nbs/hamburg/covering-a7-highway
	Hilldegarden	x		Hilldegarden bunker	8.000mq	2019-ongoing	https://una.city/nbs/hamburg/hilldegarden-city-garden-top-
Beijing	Beijing Plan area afforestation: green, urban parks and forests	x		Central Business District / City	700000000mq		https://una.city/nbs/beijing/beijing-plain-area-afforestation-
Kigali	Suncasa: afforestationr, reforestation, green, agroforestry	x		Kicukiro, Nyarugenge, and			https://www.iisd.org/suncasa/kigali
	Nyandungu Wetland Eco-park		x	Nyandungu wetland			https://una.city/nbs/kigali/nyandungu-wetland-eco-park
Singapore	Bishan-Ang Mo Kio Park & Kallang River Restoration		x	Kallang river			https://una.city/nbs/singapore/bishan-ang-mo-kio-park-
Madird	Madrid Rio: covering highway		x	Along Manzanares rio	120ha		
Milan	Vertical forest		x	Porta Nuova district	6000mq	2015	
	Parco nord		x		790ha		
	Environmental recovery of a quarry ATEg30		x	Pero	28ha		https://oppla.eu/case-study/environmental-recovery-quarry-
	Library of trees		x	Porta Nuova district	100.000mq	2016	
	Metrobosco	x			30000000mq	2006-ongoing	
Cordoba	/			/	/		
Stockholm	Tree planting		x	City centre	12.000 trees	2007	https://una.city/nbs/stockholm/fresher-city-air-green-trees
	Norra Stationsparken: urban park		x			2024	

5.3. Feasibility studies for some of the cities in the local studies

To test how to exploit ECV sequences and NBS/Urban Green Spaces information in a consistent framework, two feasibility studies have been applied to Milano and Nairobi, where the second city, while not being in the final group of the selected ones here before, is a proxy to Kigali, in the same climate zone.

5.3.1. First study: heat trends and urban greening resilience in a temperate city

To systematically characterize the resilience of urban greening and the mechanisms underlying vegetation–thermal decoupling, this study explores an integrated analytical framework. The framework comprises three interconnected stages: (1) long-term trajectory analysis and ecological memory diagnosis, to assess ecosystem stability and trend inertia; (2) detection of structural regime shifts and fine-scale disturbances, capturing both macro-level transitions and micro-level change processes in vegetation dynamics; and (3) thermal-environment retrieval and eco–thermal coupling analysis, aimed at quantifying the nonlinear thermal responses to vegetation change.

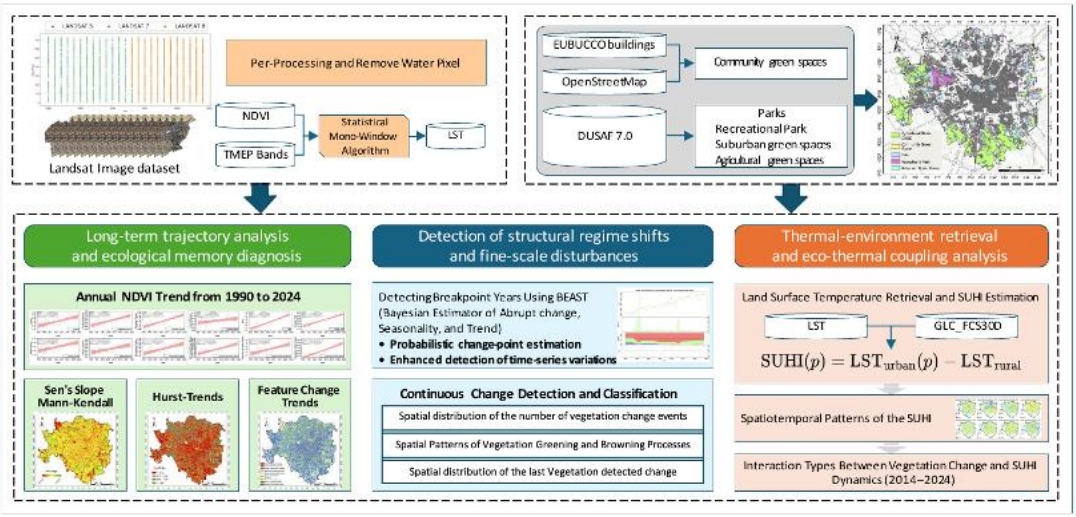

Fig. 5.1: The overall workflow of the first local study.

To characterize urban vegetation dynamics over the past three decades, an annual NDVI time series for 1990–2024. NDVI was calculated from surface reflectance, and fractional vegetation cover and emissivity were derived through:

$$FV = \frac{NDVI - NDVI_{\min}}{NDVI_{\max} - NDVI_{\min}}, \qquad \varepsilon = 0.004 \cdot FV + 0.986$$

Urban pixels were identified from the GLC-FCS30D product (class 190), while non-urban reference pixels were selected from natural land-cover classes and further constrained to lie within ±50 m of the mean urban elevation, ensuring comparable topographic conditions. Finally, SUHI intensity was computed as the difference between urban LST and the mean rural reference temperature:

$$\mathrm{SUHI}(p) = \mathrm{LST}_{\mathrm{urban}}(p) - \mathrm{LST}_{\mathrm{rural}}$$

and exported at 30-m spatial resolution for subsequent analysis.

Other than for the analysis at the finest (pixel) level, to analyze trends on the whole area, selected subareas or specific urban spaces, mean NDVI values were calculated. Compared with maximum value compositing, the mean NDVI approach better represents overall vegetation conditions and reduces potential overestimation caused by transient high-value pixels. This strategy ensures temporally consistent and comparable NDVI estimates, making it well suited for long-term urban-scale vegetation trend analysis.

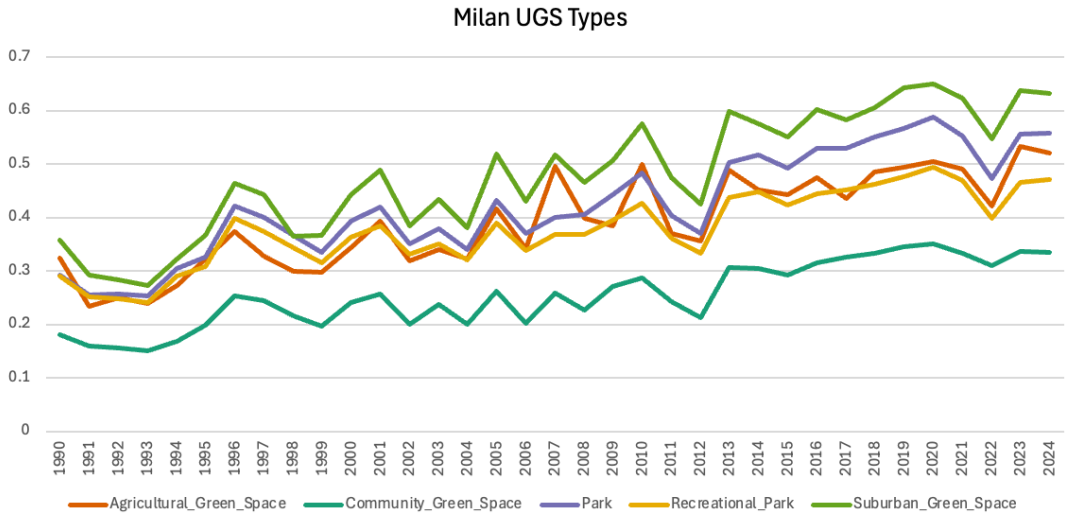

Fig. 5.2: NDVI trend for different Urban Green Space (UGS) types in Milan (1990 – 2024).

For each NDVI time series, trend magnitude and statistical significance of vegetation change were quantified using two complementary approaches at different spatial scales. At the regional scale, an Ordinary Least Squares (OLS) linear regression model was applied to estimate the annual rate of change (β_1) and the coefficient of determination (R^2) for the study area as a whole. At the pixel scale, NDVI trends were characterized using the non-parametric Theil–Sen slope estimator coupled with the Mann–Kendall (MK) test, which provides a robust assessment of trend direction and statistical significance while reducing sensitivity to outliers and distributional assumptions. The OLS regression analysis was performed assuming the following model:

$$NDVI_t = \beta_0 + \beta_1 t + \varepsilon_t$$

where t denotes the year and β_1 represents the annual rate of NDVI change.

For a given timeseries $\{ x_i(p) \}_{i=1}^{n}$ observed at times $\{ t_i \}_{i=1}^{n}$, Sen's slope is defined as the median of all pairwise slopes between time steps:

$$s(p) = \text{median}\left\{ \frac{x_j(p) - x_i(p)}{t_j - t_i} \;\middle|\; 1 \le i < j \le n \right\}.$$

where $x_i(p)$ denotes the observed value of the time series at location p and time t_i, t_i is the i-th time point in the series, and n is the total number of observations in the time series. A positive $s(p)$ indicates an increasing trend, a negative $s(p)$ a decreasing trend, while values close to zero suggest little or no change.

To objectively define the boundary between "change" and "stability," instead of conventional empirical thresholds, a bootstrap-based approach was used, explicitly accounting for the intrinsic temporal uncertainty of the observation system. This procedure was used to derive a data-driven stability threshold (ϵ_0) for the Sen's slope. Specifically, 10,000 representative pixels were randomly sampled across the study area, and each pixel-level time series was resampled 1,000 times to construct an empirical distribution of the Theil–Sen slope and to estimate the width of its 95% confidence interval (CI). The median CI width across all sampled pixels was defined as the minimum detectable magnitude of change. Pixels with slope magnitudes satisfying $|s| \le \epsilon_0$ were classified as stable, whereas values exceeding this threshold were interpreted as indicating physically meaningful vegetation change.

Once the direction and magnitude of the trend were determined, its statistical significance was assessed using the non-parametric Mann–Kendall test. This approach does not assume any underlying distribution and is relatively insensitive to outliers, making it well suited for time-series RS data. Trend significance is evaluated using the standardized statistic Z, defined as:

$$Z = \begin{cases} \dfrac{S-1}{\sqrt{\mathrm{var}(S)}}, & S > 0, \\ 0, & S = 0, \\ \dfrac{S+1}{\sqrt{\mathrm{var}(S)}}, & S < 0. \end{cases}$$

At a significance level α, the trend is assessed using the standard normal distribution when $|Z| > Z_{1-\alpha/2}$. A trend is considered significant at the 95% confidence level when $Z \geq 1.96$. The $sgn(\cdot)$ and the variance term $\mathrm{Var}(S)$ are defined as follows:

$$\mathrm{sgn}(x) = \begin{cases} 1, & x > 0, \\ 0, & x = 0, \\ -1, & x < 0. \end{cases}$$

If tied values occur within the series, the variance is adjusted as:

$$\mathrm{Var}(S) = \frac{n(n-1)(2n+5) - \sum_{k=1}^{m} t_k\,(t_k-1)(2t_k+5)}{18},$$

where the m denotes the number of tie groups; t_k is the number of observations in the k-th group; If no ties are present, then $\sum_{k=1}^{m} t_k\,(\cdots) = 0$, and the expression reduces accordingly.

Beyond describing historical trends, ecological memory and potential future trajectories were evaluated using the Hurst exponent (H). While Sen's slope and the Mann–Kendall test quantify the direction and significance of past trends, they do not indicate whether these trends are likely to persist or reverse. To address this limitation, H was calculated to characterize the long-term memory of the NDVI time series based on rescaled range analysis. Values of $H > 0.5$ indicate persistent behavior, $H = 0.5$ corresponds to a memoryless random process, and $H < 0.5$ denotes anti-persistence, implying an increased likelihood of trend reversal. This metric therefore provides a probabilistic basis for distinguishing sustainable greening from potentially reversible vegetation trajectories.

To further differentiate the strength of persistence, H is classified into four categories: (i) 0–0.35: strong anti-persistence; (ii) 0.35–0.50: weak anti-persistence; (iii) 0.50–0.65: weak persistence; (iv) $>$ 0.65: strong persistence.

By combining Hurst classes with the sign of Sen's slope, the likely future trajectory and stability of NDVI change can be inferred, thereby providing a forward-looking assessment of urban vegetation dynamics.

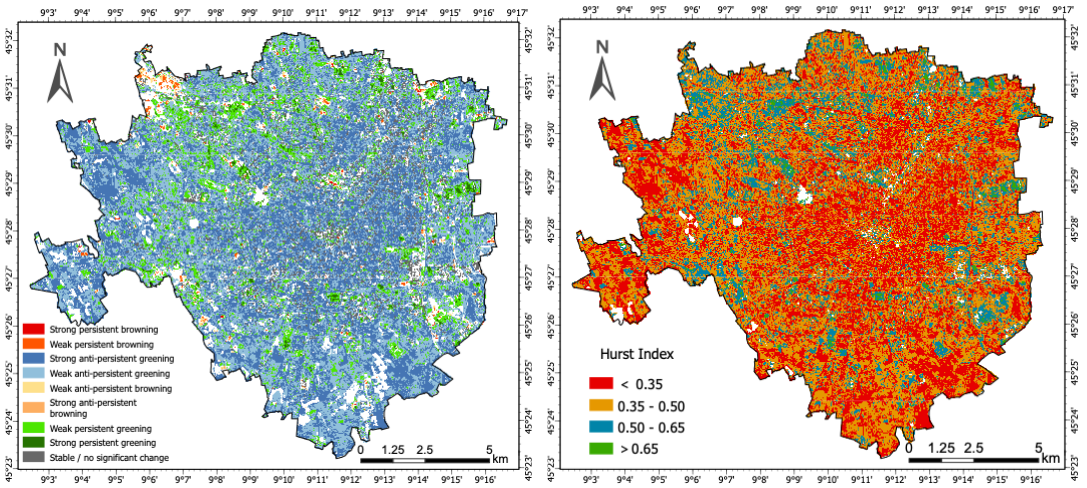

Fig. 5.3: Long-term NDVI trends, persistence, and future trajectory classification from 1990–2024 in Milano.

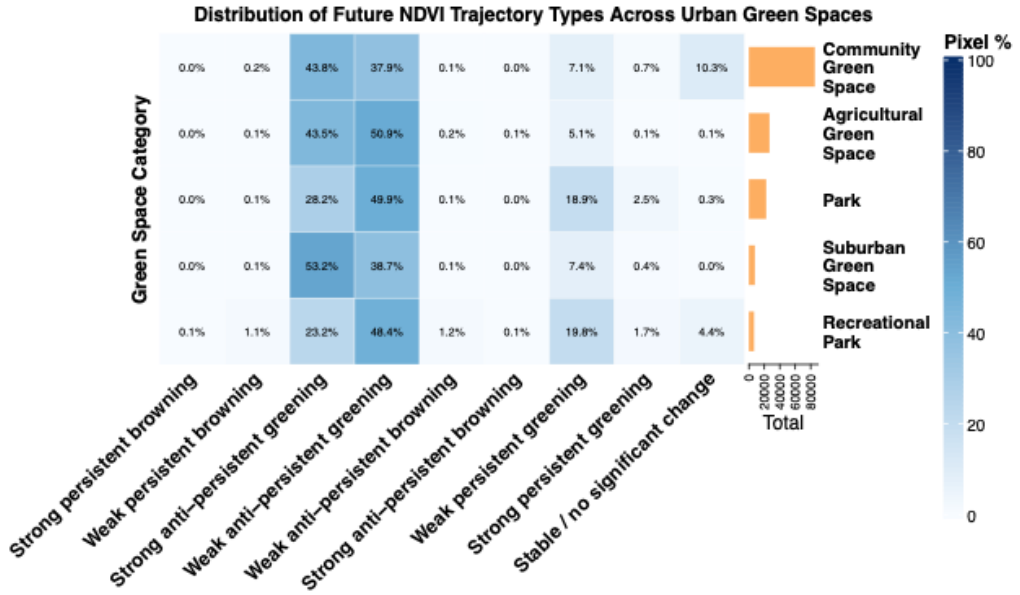

Fig. 5.4: Distribution of future NDVI trajectory type across UGSs.

Class	Sen's slope s	Hurst H	Interpretation
1	$s < -0.0021$	$H > 0.65$	Strongly persistent degradation
2	$s < -0.0021$	$0.50 < H < 0.65$	Weakly persistent degradation
3	$s \geq 0.0021$	$0 < H < 0.35$	Strong anti-persistent greening
4	$s \geq 0.0021$	$0.35 < H < 0.50$	Weak anti-persistent greening

Class	Sen's slope s	Hurst H	Interpretation
5	$s < -0.0021$	$0.35 < H < 0.50$	Weak anti-persistent degradation
6	$s < -0.0021$	$0 < H < 0.35$	Strong anti-persistent degradation
7	$s \geq 0.0021$	$0.50 < H < 0.65$	Weakly persistent greening
8	$s \geq 0.0021$	$H > 0.65$	Strongly persistent greening
9	$\|s\| \leq 0.0021$	any H	Stable / no significant long-term change

To capture non-stationary dynamics beyond linear trends, two complementary time-series segmentation approaches were jointly considered. Specifically, the BEAST model was employed to identify regime-shift timing at the regional scale, while the CCDC algorithm was applied to reconstruct pixel-level disturbance histories and spatial turnover patterns.

As the regional-scale component of the non-stationary time-series analysis, the BEAST model was employed to probabilistically identify the timing and magnitude of regime shifts in NDVI and SUHI trajectories. BEAST decomposes an observed time series y_t into trend, seasonal, and noise components as follows:

$$y_t = T_t + S_t + \varepsilon_t$$

while allowing the trend and seasonal terms to contain an unknown number of breakpoints. These breakpoints, together with their timing and magnitude, are inferred probabilistically through a Bayesian framework using MCMC sampling. The model therefore jointly estimates long-term trends, seasonal patterns (when present), and the probability of abrupt shifts, providing a coherent representation of both gradual and sudden changes in the series.

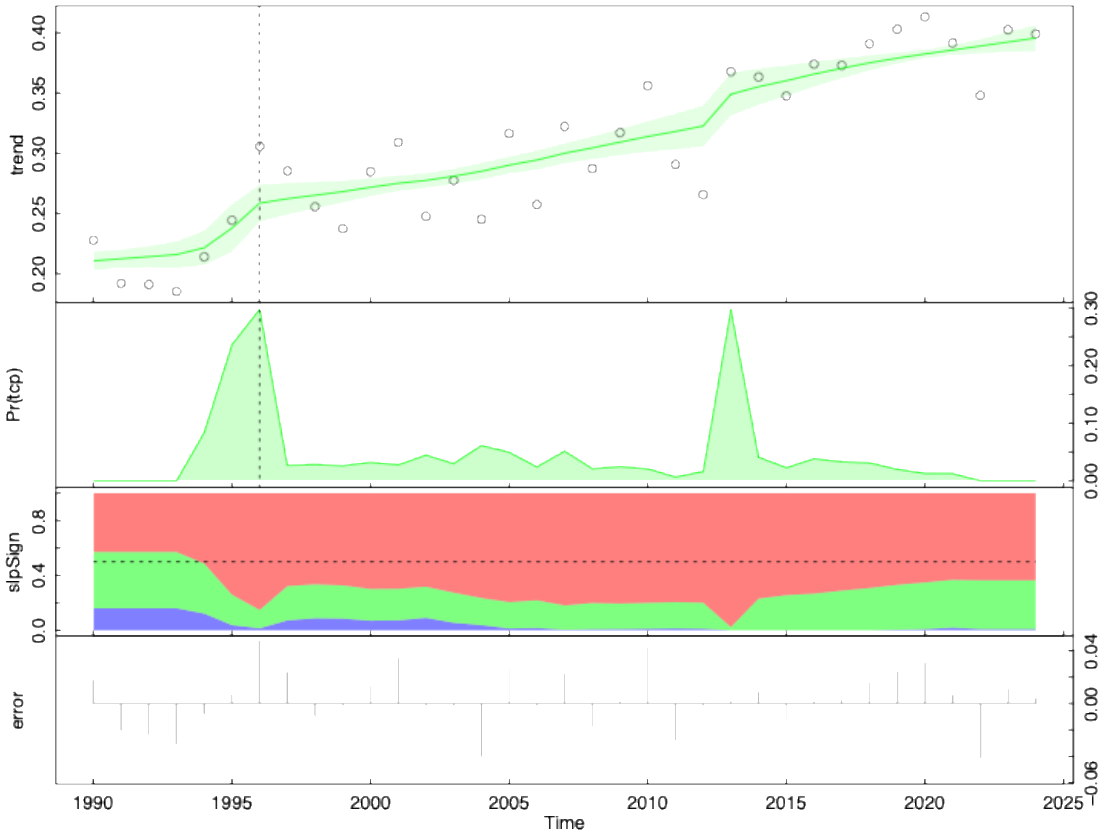

Fig. 5.5: BEAST decomposition and change point detection of the annual NDVI series (1990 – 2024).

Moreover, to characterize continuous vegetation dynamics and fine-scale disturbance–recovery processes, the Continuous Change Detection and Classification (CCDC) algorithm was applied. CCDC fits harmonic regression models to surface reflectance time series and detects structural breaks by monitoring residuals relative to predefined thresholds. For each pixel, the model represents the spectral signal as:

$$y_t = \beta_0 + \beta_1 t + \sum_{i=1}^{k} [a_i \cos(\omega\, 2\pi i t) + b_i \sin(\omega\, 2\pi i t)] + \varepsilon_t$$

where $\beta_0 + \beta_1 t$ captures the long-term trend, the harmonic terms describe seasonal variability, ω denotes the annual cycle, and ε_t represents noise. Breaks are identified when model residuals exceed the confidence bounds, indicating a significant deviation from the expected trajectory.

The CCDC operates continuously through time and can detect both abrupt and gradual changes, offering higher temporal sensitivity than single-date or sparse multi-temporal approaches. In this study, CCDC outputs were used to extract the timing and spatial distribution of major vegetation shifts, providing pixel-level

detail alongside the regime-shift information derived from BEAST. Together, they provide a robust and temporally resolved depiction of NDVI evolution, enabling a more accurate interpretation of long-term greening, browning and disturbance–recovery processes.

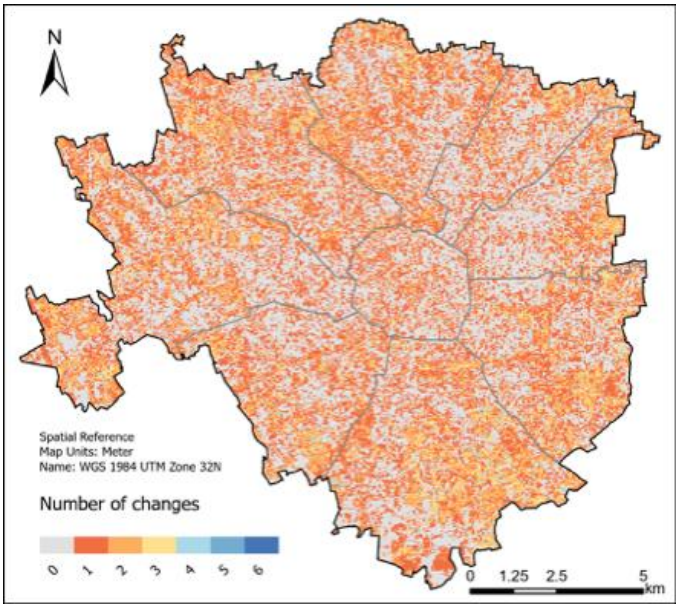

Fig. 5.6: Spatial distribution of the number of vegetation change events identified by CCDC in Milan.

Finally, to highlight the nonlinear eco–thermal coupling between vegetation dynamics and urban heat-island evolution, a trend-based bivariate classification approach that jointly analyses long-term NDVI and SUHI trajectories to delineate distinct eco–thermal response pathways was implemented. Specifically, based on the trend magnitude (obtained by Theil–Sen slopes) and statistical significance (assessed using the Mann–Kendall test), univariate trajectories were initially classified into five categories: significant browning / cooling, non-significant browning / cooling, stable, non-significant greening / intensification, and significant greening / intensification. For the purpose of bivariate analysis, these five states were further aggregated into three dominant directional classes by pooling both significant and non-significant decreases as “Browning/Cooling”, retaining stable conditions as “Stable”, and pooling both significant and non-significant increases as “Greening/Intensification”.

NDVI trajectories were subsequently consolidated into three ecological states — greening, stable, and browning— whereas SUHI trajectories were classified into three thermal states: cooling, stable, and intensification. Overlaying these classifications yielded a 3×3 eco–thermal response matrix with 9 joint trajectory types (see next table). This approach enables the identification of areas where vegetation change and thermal response are functionally decoupled, thereby

revealing pronounced spatial heterogeneity in the heat-mitigation performance of urban green spaces.

The nine-class eco–thermal trajectory types obtained by overlaying NDVI and SUHI three-state layers.

NDVI state \ SUHI state	Cooling (Down)	Stable	Intensification (Up)
Browning (Down)	Browning–Cooling	Browning–Stable	Browning–Intensification
Stable	Stable–Cooling	Stable–Stable	Stable–Intensification
Greening (Up)	Greening–Cooling	Greening–Stable	Greening–Intensification

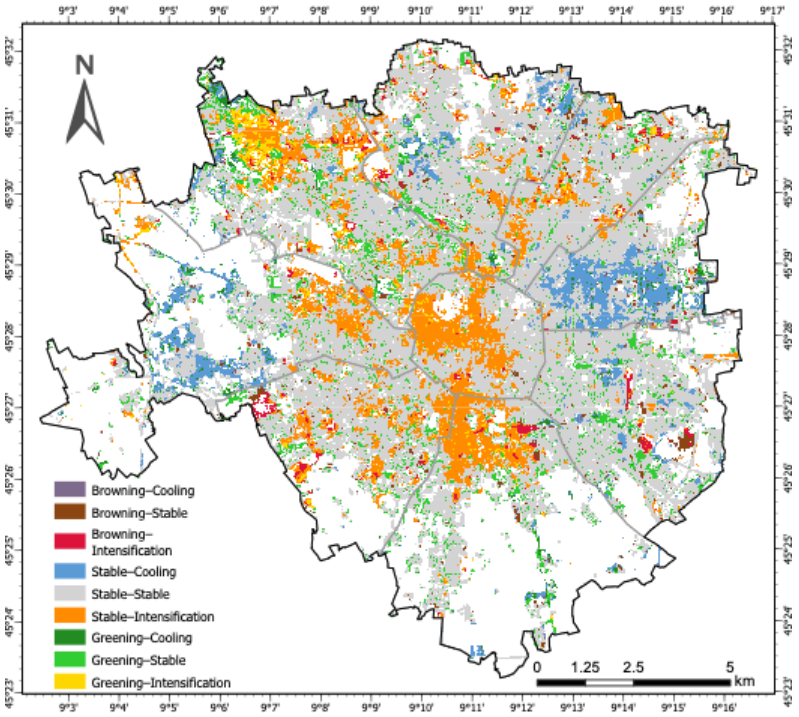

Fig. 5.7: Joint trajectories of NDVI and SUHI trends in Milan for the period 2014 – 2024.

5.3.2. Second study: morphology (LCZ) stratified thermal contrasts in a tropical city

This second study is preliminary analysis of the impact or urban morphology on thermal emissions and thermal vulnerability in two African cities characterized by extensive areas of informal settlements, Nairobi and Eldoret (Kenya).

In this case, urban morphology is represented using Local Climate Zone (LCZ) maps produced independently. Specifically, in this study, LCZ maps are treated as fixed contextual inputs and are used to guide material-aware emissivity correction in lightweight informal settlements (LCZ 7).
Indeed, field measurements reported by Nichol et al. [11] indicate that corrugated metal and oxidate iron roofing dominant materials in LCZ 7 settlements exhibit

substantially lower thermal infrared emissivity than typical formal urban materials, generally ranging from 0.65 to 0.83 depending on oxidation and surface condition. Based on these observations, the following formula was adopted to compensate in these areas for this phenomenon:

$$T_{\text{corrected}} = \frac{T_{\text{Landsat}}}{1 + \left(\frac{\lambda T_{\text{Landsat}}}{\rho}\right) \ln\left(\frac{\varepsilon_{\text{LCZ7}}}{\varepsilon_{\text{Landsat}}}\right)}$$

where λ = 10.8 μm (effective wavelength of Landsat TIRS Band 10), ρ = 1.438 × 10−2 m K, ε_{LCZ7} = 0.83, and $\varepsilon_{Landsat}$ ≈ 0.96. All non-LCZ 7 pixels retain their original Landsat LST values to preserve baseline thermal relationships across vegetation, water, and formal urban surfaces. A dominance threshold of 0.75 was used to ensure that emissivity correction is applied only where LCZ 7 materials dominate the thermal signal. The 0.75 threshold ensures that at least three-quarters of the thermal pixel corresponds to LCZ 7 materials, minimizing mixed-pixel contamination while maintaining sufficient sample size.

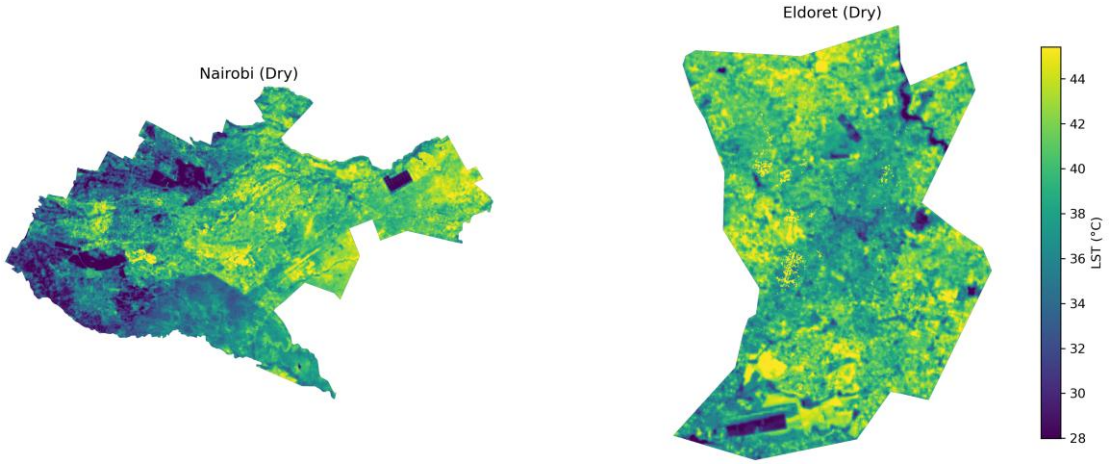

Fig. 5.8: Land surface temperature for Nairobi and Eldoret during the dry season.

After correction, LCZ-wise aggregation of the 10 m LST fields confirms systematic thermal differences linked to urban morphology (see next Table). Across both cities, LCZ 7 (informal settlements) consistently exhibits the highest temperatures, exceeding LCZ 3 by 3.1–6.8 K depending on city and season. Nairobi shows stronger LCZ separation than Eldoret, reflecting its denser urban fabric.

Table 5.2: Mean LST (°C) by Local Climate Zone (LCZ) for Nairobi and Eldoret.

LCZ	Nairobi Dry	Nairobi Wet	Eldoret Dry	Eldoret Wet
LCZ 3 (Compact low-rise)	40.61	40.72	39.72	35.69

LCZ 7 (Lightweight low-rise)	46.61	47.55	43.03	38.83
LCZ 8 (Large low-rise)	42.44	42.92	38.88	32.42
LCZ 10 (Heavy industry)	40.87	40.92	39.89	35.36
Natural LCZs (A–G, mean)	37.34	35.40	39.03	30.29
LCZ7 - LCZ3	**6.01**	**6.83**	**3.31**	**3.14**

6. Assessment of the added value of EO to the science challenge

The EO data that will be exploited for the scope of this project cover three main categories: urban morphology, climate and NBS proxies. These categories are directly aligned with the project's objective to analyze urban climate–NBS interactions across cities and over time, by combining information on urban structure, surface properties, and thermal response

Urban morphology

The 3D characteristics of the building stock have a strong influence on the local climate condition and resilience, respectively. However, globally available data describing the building shape, height and arrangement within the built-up area remain rare. To close this gap, we employ the World Settlement Footprint 4D (WSF® 4D) dataset that merges regionally existing state-of-the-art building footprint datasets and assigns information on area, height, volume, and year of construction to each building. Comprising a total of 2.7 billion footprints, the resulting dataset represents one of the most accurate and complete open global building inventories available to date. At the same time, the WSF® 4D is the first dataset to describe the global growth pattern of the building stock over the last four decades. The WSF® 4D also gives a detailed overview of remaining gaps in the spatial coverage of the settlement area with footprint data. The WSF® 4D thus provides a significantly enhanced evidence base to enable more detailed and accurate assessments of the statistical relationship between urban morphology and climate conditions and resilience across global cities.

From an EO perspective, the added value lies in the ability to derive spatially explicit and globally consistent information on urban structures, which is not available from climate or model-based datasets. At the same time, limitations remain in terms of data completeness, temporal updating, and potential regional inconsistencies in input sources, which may affect cross-city comparability.

Climate

EO-based Land Surface Temperature (LST) represents the primary variable for observing urban thermal conditions. Long-term datasets such as ESA CCI LST and Copernicus Climate Data Store (~1 km) provide globally consistent, multi-decadal observations suitable for trend analysis and inter-city comparison. EO-based LST also enables the derivation of standardized indicators such as the Surface Urban Heat Island (SUHI), which can be computed in a consistent manner across cities, supporting robust inter-city comparison. In addition, the availability of long-term EO records allows the analysis of temporal trends in urban thermal conditions, which is critical for assessing changes over time at global scale.

The main added value of EO lies in the direct observation of the surface thermal signal, enabling spatially explicit analysis of urban climate patterns across scales. However, coarse-resolution datasets do not capture fine-scale variability, while higher-resolution products lack temporal consistency and global coverage. In addition, LST reflects a composite signal influenced by urban morphology and meteorological conditions, which limits the attribution of observed thermal patterns to specific drivers. Other variables, such as air temperature and precipitation, are typically derived from reanalysis or model-based products to provide contextual information.

This highlights the role of EO-based LST as a unique variable for linking spatial patterns of surface properties with their thermal response, while also underlining the need for complementary data to support interpretation.

NBS proxies

EO-based land surface and vegetation datasets provide spatially explicit information on vegetation presence and structure, which can be used as proxies for the distribution and intensity of Nature-Based Solutions (NBS). Global datasets such as ESA WorldCover (~10 m), CCI Biomass (~100 m), and LAI products (~300 m–1 km) enable consistent characterization of vegetated versus impervious surfaces across cities.

Similarly, the availability of repeated EO observations enables the analysis of temporal dynamics in vegetation conditions (e.g., seasonal variability and long-term trends), which can support the analysis of how changes in vegetation patterns relate to observed thermal trends. However, differences in temporal resolution and data continuity across datasets may limit the robustness of such analyses.

At finer scales, Sentinel-2 (~10 m) supports the derivation of greenness indicators (e.g., NDVI) and imperviousness fractions, improving the representation of intra-urban variability.

The added value of EO lies in the ability to map vegetation consistently across spatial scales within a unified observational framework. However, these variables represent indirect proxies of NBS and do not capture their typology, design, or functionality. Differences in spatial resolution, temporal frequency, and classification schemes across datasets may also affect consistency and comparability, particularly in cross-city analyses.

In this context, EO provides a consistent and scalable approach to represent vegetation-related processes, but the interpretation of these proxies in terms of actual NBS performance remains inherently limited.

Across the three categories, EO datasets provide a unique capability to observe urban morphology, vegetation, and thermal response within a consistent spatial framework. This enables analyses across scales, from global inter-city comparison to local intra-urban assessment, although trade-offs exist between spatial resolution and temporal consistency. At the same time, differences in spatial resolution, temporal coverage, and variable definition across datasets introduce challenges for consistency and interpretation. In particular, the combined use of morphology, NBS proxies, and LST supports the identification of spatial patterns and relationships, while the attribution of observed effects to specific processes remains subject to uncertainty.

Overall, this combination of EO datasets provides the basis for addressing the project's core scientific challenge, namely the consistent assessment of relationships between urban morphology, vegetation patterns, and thermal response across cities and over time, while acknowledging the limitations in causal attribution.

7. Uncertainties in the proposed scientific studies

The scientific studies proposed within MOMO-NBS are methodologically ambitious and span two complementary spatial scales: a global comparative study covering 159 cities and a local intra-city monitoring study covering 10 case study cities. Both studies depend on the consistent integration of ECVs, 2D/3D morphological indicators, and NBS characterization derived from EO data.

7.1. Uncertainties in successfully achieving the scientific objectives

Four categories of uncertainty have been identified as relevant to global and local studies. Their interaction is summarized in Table 7.1 and detailed in the subsections below.

Table 7.1. Summary of uncertainty sources, affected variables, indicative magnitudes, and mitigation approaches.

Uncertainty type	Affected variables / analyses	Indicative magnitude	Quantification approach	Reduction / mitigation strategy
Product-level (resolution & coverage)	LST (CCI 1 km; ECOSTRESS 70 m); Albedo (300 m–1 km); AGB (100 m); all ECV-based climate indicators	SUHI bias of ±0.5–2 K at 1 km vs. 70 m; albedo signal integration across mixed surfaces	Resolution sensitivity tests: compare SUHI estimates derived from CCI LST vs. ECOSTRESS vs. Landsat (30 m) for a subset of cities; report divergence metrics	LST downscaling using statistical/deep-learning methods where applicable (see §7.2.1); Systematic use of 10 m imperviousness/greenness and LoD1 building model as surface-characterization bridge;
Scale-mismatch & temporal inconsistency	LST cross-product fusion (CCI + ECOSTRESS + Landsat); land cover thematic harmonization; LAI products (300 m–1 km) vs. Sentinel-2 NDVI (10 m)	Cross-product LST difference of 1–3 K in complex urban morphologies; thematic class disagreement rate of 5–20% across cities	Explicit uncertainty propagation when fusing LST products; inter-product classification agreement matrix for NBS-relevant land cover classes	Dual-product LST strategy (CCI for trends; ECOSTRESS/Landsat for local attribution); consistent thematic reclassification protocol across all cities (see §7.2.2)
Attribution & thematic uncertainty	LST-NBS attribution in global and local studies; NBS classification comparability across 10 cities; LCZ-stratified thermal contrasts	Multi-factor LST variation of 3–7 K attributable to morphology, materials, and vegetation combined; NBS class disagreement across national inventories	LCZ-stratified analysis to disaggregate thermal signal by morphological class; NBS classification sensitivity tests with alternative typologies in subset cities; report attribution confidence per city	Morphological stratification framework (LCZ); harmonized NBS typology (4 classes) cross-validated against stakeholder inventories; co-design consultation protocol (see §7.2.3 and §7.2.5)
Data availability & coverage gaps	LoD1 building model completeness; OSM contributor density; NBS inventory	Coverage gaps in Africa and parts of Asia; OSM building tagging quality varies; NBS inventory	Document coverage completeness metrics per city; report WSF 4D gap flags; track NBS inventory	Tiered fallback data strategy; deep learning model for building height at 10 m; structured stakeholder consultation protocol; tiered attribution confidence

Uncertainty type	Affected variables / analyses	Indicative magnitude	Quantification approach	Reduction / mitigation strategy
	completeness; Global South cities (Kigali, Manila)	sparse in some cities	confidence level per city	reporting (see §7.2.4 and §7.2.6)

7.1.1. Spatial resolution limitations of available ECVs

Most ECV products in the D1.3 inventory operate at spatial scales that cannot resolve individual NBS features (see Section 3.3 for scoring details). LST products span from 70 m (ECOSTRESS, 8-year record) to 1 km (CCI LST, 31-year record); albedo products are available only at 300 m to 1 km; surface radiation budget and precipitation products at 5.5 to 25 km; and all greenhouse gas products remain at spatial score 1 under the DLR framework (Table 3.1).

This resolution gap is more consequential for the local study, where small-scale NBS interventions, street trees, green roofs, and retention ponds, fall below the detection threshold of the available ECV stack. The gap manifests as a systematic underestimation of intra-urban thermal contrasts at the pixel scale, and as an inability to attribute observed signals to specific NBS features without high-resolution ancillary support. For LST, resolution sensitivity tests conducted during the Milan and Nairobi feasibility studies (Section 5) demonstrate that SUHI intensity derived at 30 m (Landsat) and at 1 km (CCI LST) can diverge by 0.5 to 2 K in morphologically complex areas, with larger divergences in compact high-rise and informal settlement zones.

For the global study, resolution limitations are less critical because the analysis operates on zonal statistics aggregated across urban extent and concentric rings; however, coarse ECV products introduce uncertainty into the ring-level LST estimates, particularly for the innermost rings of cities with heterogeneous morphologies.

Coverage gaps compound resolution limitations in certain regions. LST IR products accumulate significant data gaps due to cloud cover, with coverage rates varying substantially by climate zone and season, tropical cities in particular face systematic gaps during wet seasons. Albedo products are similarly cloud-affected. For above-ground biomass, the use of BIOMASS CCI in urban areas requires additional caution due to potential radar and LiDAR interference from urban infrastructure, which may introduce systematic biases in densely built environments.

Note: *See Section 4.2.4 for the specific statistics and gap-management approaches planned for the urban climate characterization. See Section 7.2.1 for the mitigation strategy.*

7.1.2. Scale mismatch and temporal inconsistency between data products

Scale-mismatch uncertainty arises when products of different spatial support are combined within the same analytical workflow. Even a high-quality ECV product may contribute uncertainty if its pixel integrates multiple urban surface types that differ in their thermal or radiative behavior. This is particularly relevant for LST, where a 1 km pixel in a compact mid-rise city such as Milan integrates formal built surfaces, street canyons, courtyards, and tree canopy simultaneously.

Temporal-consistency uncertainty is the complementary problem: the finest-resolution products available for local attribution tend to have shorter records, lower temporal continuity, or more limited spatial coverage than coarser long-term products. For LST, ECOSTRESS (70 m) covers only 8 years and its acquisitions are not evenly distributed through the diurnal cycle or across seasons, which can introduce thermal bias in comparative analyses across cities or years. Combining ECOSTRESS with CCI LST (1 km, 31 years) therefore introduces cross-product uncertainty from differing retrieval assumptions, sensor viewing geometries, and temporal sampling strategies.

Land cover products show the most favorable multi-resolution stack with WorldCover (10 m) and CLCplus (10-30 m) providing adequate spatial support, but thematic harmonization across cities remains a challenge, as classification schemes and NBS-relevant classes are not consistently defined across the available products Several land cover products do not include an explicit uncertainty layer, which limits the propagation of classification confidence into downstream analyses.

For vegetation-related products, CCI Biomass at 100 m offers a reasonable compromise for neighborhood-scale interpretation, but LAI products at 300 m to 1 km resolution cannot capture the small-scale vegetation interventions, for example, a dense urban park from scattered street trees in a compact low-rise zone.

Note: *See Section 3.3 for the full uncertainty typology and Table 3.3 for product-level details. See Section 7.2.2 for the mitigation strategy.*

7.1.3. Attribution uncertainty in linking ECV signals to NBS

Urban LST patterns are simultaneously shaped by urban density, building height, surface materials, street-canyon geometry, vegetation presence, imperviousness, wind exposure, and meteorological background conditions. The observed thermal signal at any given location is therefore a composite of multiple co-varying factors, and disentangling the contribution of NBS from this multi-factor signal is one of the central scientific challenges of the local study.

Attribution uncertainty takes a specific form in cities where NBS are embedded within morphologically complex urban fabrics. For Instance, in Milan's compact mid-rise structure, a greening signal in NDVI may reflect the expansion of a rooftop garden, a courtyard tree, or a change in street-level imperviousness, each

of which would have different thermal implications and spatial extents. In Singapore's high-density tropical setting, multiple co-varying factors such as building height, vegetation canopy, reflective materials, and the urban moisture regime contribute to the ECV signal simultaneously.

In the global study, attribution uncertainty takes a different form: statistical relationships between 3D urban form and ECV-derived climate indicators may capture compounding effects driven by climate zone, topographic setting, or socioeconomic context across the 159-city sample, rather than by morphology alone. The stratified sampling design based on Köppen-Geiger climate zones, urban morphotype, topography, and level of socioeconomic development partially addresses this, but residual confounding from unobserved variables cannot be fully eliminated through observational design alone.

Thematic uncertainty also arises from the absence of a universally agreed NBS definition and from the wide variation in how urban greening, Blue-Green Infrastructure, Green Stormwater Infrastructure, and natural vegetation are classified across national planning systems. Cities that use different terminology or classification criteria produce datasets that are not directly comparable without harmonization, which introduces a second layer of thematic uncertainty into the cross-city analysis.

Note: *See Section 4.2.3 for the greenness/imperviousness product logic and its uncertainty sources. See Section 4.2.4 for the urban climate characterization approach. See Section 7.2.3 and 7.2.5 for mitigation strategies.*

7.1.4. Data availability and stakeholder engagement gaps

For cities in the Global South (e.g., Kigali and Manila) high-resolution ancillary EO layers (LoD1 building model, 10 m imperviousness/greenness layer) may have incomplete coverage, variable accuracy, and lower OSM contributor density than European cities. These layers are critical inputs for reducing scale-mismatch uncertainty; their incompleteness therefore propagates directly into the attribution confidence of the local study in the cities where high-resolution anchoring is most needed.

NBS inventory completeness mirrors this asymmetry. Cities such as Hamburg, Stockholm, and Milan bring established institutional connections, existing NBS inventories, and mature urban greening policies to the co-design process. In contrast, Kigali and Córdoba are at earlier stages of NBS planning and data documentation, and some stakeholders have not yet provided responses to consultation requests. Where locally validated NBS location data are absent or sparse, the ability to confirm or refute ECV-based NBS characterization is reduced.

The consequence is not merely a project management challenge but a scientific one: data availability gaps introduce differential uncertainty across cities, which must be explicitly documented and accounted for in cross-city comparisons. Results for cities with sparse ancillary data should be interpreted with lower attribution confidence than results for cities with complete data stacks.

Note: *See Section 7.2.4 and 7.2.6 for the tiered fallback data strategy and stakeholder consultation protocol.*

7.2. Quantification and mitigation of uncertainties

For each uncertainty source identified in Section 7.1, Table 7.2 below summarizes the planned quantification method, the reduction strategy, and the residual uncertainty that is expected to remain after mitigation. The subsections that follow provide methodological detail on each strategy. Where the relevant methodological approach has already been described in another section of this document, the discussion here is limited to the uncertainty-specific aspects and a cross-reference is provided.

Table 7.2. Uncertainty quantification methods, reduction strategies, and residual uncertainty by uncertainty source.

Uncertainty source	Quantification method	Reduction strategy	Residual uncertainty
Resolution gap in LST products	Resolution sensitivity tests comparing SUHI derived from CCI LST (1 km), Landsat (30 m), and ECOSTRESS (70 m) for a representative subset of cities; divergence statistics reported	10 m imperviousness/greenness and LoD1 building model used as surface-characterization bridge; LST downscaling applied where feasible; results reported with product-specific confidence flags	Irreducible for small NBS features (<70 m); explicitly documented in results interpretation
Cross-product LST fusion uncertainty	Uncertainty propagated explicitly when combining CCI LST and ECOSTRESS; sensor differences, viewing geometry offsets, and retrieval algorithm divergence documented per city	Dual-product strategy: CCI LST for long-term baseline; ECOSTRESS and Landsat LST for local attribution window; products not directly fused unless uncertainty is quantified first	Cross-sensor LST bias of 0.5–2 K in dense urban fabrics; reported as uncertainty range on SUHI estimates
Land cover thematic inconsistency	Inter-product classification agreement matrix computed for NBS-relevant classes (vegetation, impervious, water, hybrid) across all 10 cities; disagreement rates reported per city	Consistent thematic reclassification protocol applied across WorldCover, CLCplus, and local datasets; NBS-relevant classes defined a priori and applied uniformly (see §4.2.3)	Residual thematic disagreement of 5–15% expected in cities lacking locally validated reference data
Attribution of LST to NBS vs. confounding factors	LCZ-stratified analysis used to disaggregate thermal signal by morphological class; sensitivity of attribution to alternative LCZ boundaries tested; attribution confidence reported per city	Morphological stratification framework (LCZ) reduces confounding from mixed surface types; LCZ classification produced from morphological and spectral inputs where not	Multi-factor confounding irreducible without randomized experimental design; residual attribution uncertainty explicitly stated in findings

Uncertainty source	Quantification method	Reduction strategy	Residual uncertainty
		already available (see §7.2.3)	
NBS classification inconsistency across cities	NBS classification sensitivity tests: alternative typologies applied to subset of cities; disagreement rate between local inventories and harmonized typology reported	Harmonized 4-class NBS typology adopted (large parks/forests; street trees/small greenery; blue infrastructure; hybrid blue-green elements); cross-validated against stakeholder inventories where available	Residual comparability limitations for cities with sparse or undocumented NBS inventories; reported as confidence tier in cross-city results
EO data coverage gaps (Global South)	WSF 4D gap flags and OSM tagging quality metrics documented per city; NBS inventory completeness score assigned to each local-study city	Alternative strategy: deep learning model for building height at 10 m resolution; structured stakeholder consultation to supplement sparse local data (see §7.2.4 and §7.2.6)	Uneven analytical depth across cities acknowledged; Global South cities assigned lower attribution confidence tier where data gaps persist

7.2.1. Mitigation of Spatial Resolution Limitations

The primary strategy for addressing the spatial resolution gap is the systematic use of the 10 m imperviousness/greenness layer derived from Sentinel-2 (Section 4.2.3) and the LoD1 building model combining footprint, height, volume, and construction year (Section 4.2.2). These layers provide detailed surface characterization that can be used to contextualize, disaggregate, and validate ECV-based signals at finer spatial scales than the ECV products themselves permit.

Resolution sensitivity tests will be conducted for a representative subset of cities by comparing SUHI estimates derived independently from CCI LST (1 km), Landsat LST (30 m), and ECOSTRESS (70 m). The divergence statistics from these tests will be reported and used to assign product-specific confidence flags to the local attribution results. Where divergence exceeds a predefined threshold, results will be reported as indicative rather than quantitative.

For the global study, zonal statistics aggregated across the urban extent and the five concentric rings partially reduce pixel-level resolution effects. For the local study, LST downscaling using statistical or deep-learning techniques will be applied where available training data permit, following the approach demonstrated in the Milan and Nairobi feasibility studies.

Coverage gaps in LST and albedo products due to cloud cover will be managed through temporal compositing strategies (e.g., seasonal composites rather than monthly means for cloud-prone cities) and by using difference-based metrics between urban zones rather than absolute values, which are less sensitive to missing data than absolute trend estimates.

7.2.2. Mitigation of Scale Mismatch and Temporal Inconsistency

To address the resolution–record-length trade-off in LST, the project adopts a dual-product strategy. CCI LST (1 km, 31 years) serves as the long-term climatological baseline for trend analysis and inter-city comparison. ECOSTRESS (70 m, 8 years) and Landsat-derived LST (30 m) provide finer spatial detail for intra-urban NBS attribution within the most recent analysis window. Products are not directly fused without prior uncertainty quantification: where cross-product comparison is required, uncertainty introduced by differing sensor characteristics, viewing geometries, and retrieval algorithms will be explicitly documented and propagated through the analysis as uncertainty bands on the reported metrics.

The ECOSTRESS temporal sampling gap, the non-uniform distribution of acquisitions across the diurnal cycle and seasons, is partially managed by supplementing with Landsat-derived LST, which provides a more consistent temporal sampling for the daytime overpass window. Seasonal compositing will be used to reduce the influence of individual acquisition anomalies.

For land cover, temporal harmonization will be achieved by selecting products whose classification periods are aligned with the NBS implementation timelines available from stakeholder data, and by applying consistent thematic reclassification protocols across all cities. An inter-product classification agreement matrix will be computed for NBS-relevant land cover classes across all 10 local-study cities, and disagreement rates will be reported per city as a transparency measure. The lack of explicit uncertainty layers for several land cover products will be partially compensated by cross-validating product classifications against locally validated reference datasets where available.

Note: *For the detailed description of ECV selection and processing for the urban climate characterization, see Section 4.2.4. For the greenness/imperviousness product, see Section 4.2.3.*

7.2.3. Mitigation of Attribution Uncertainty

Attribution uncertainty will be addressed through the morphological stratification framework, whereby ECV signals are analyzed within LCZ-defined urban surface classes rather than in an undifferentiated urban mask. This approach, demonstrated in the Nairobi/Eldoret feasibility study (Section 5.2), allows the thermal signal to be disaggregated by morphological class, reducing the confounding effects of mixed urban surface types. LCZ-stratified results are then compared across cities to assess whether the same morphological class produces consistent thermal behavior in different climate zones, providing a basis for separating morphological from climatic drivers.

The sensitivity of attribution results to alternative LCZ boundary definitions will be tested for a subset of cities by applying alternative classification inputs and comparing the resulting LCZ-stratified LST contrasts. Attribution confidence will be reported per city as a tiered indicator: high confidence where LCZ maps are available at sufficient detail, stakeholder-validated NBS inventories are complete, and cross-product LST agreement is within acceptable bounds;

medium confidence where one of these conditions is not met; and low confidence where two or more conditions are not met.

In cities where LCZ maps are not yet available at sufficient spatial detail, LCZ classification will be produced from available morphological and spectral inputs as part of the data tailoring workflow described in D2.2.

7.2.4. Mitigation of Stakeholder Engagement Risks

To reduce the risk of uneven stakeholder engagement, the project consortium will maintain direct institutional connections to local partners in each of the 10 case study cities. For cities where formal NBS planning documents are limited, the co-design process will be supported by a structured consultation protocol, including targeted workshops, questionnaires, and iterative review of preliminary results, to ensure that local actors contribute to both the NBS characterization and the interpretation of ECV-based findings.

The scientific consequence of incomplete stakeholder engagement is a reduction in NBS inventory completeness, which in turn limits the ability to validate ECV-based NBS characterization. This consequence will be made explicit in the analysis by assigning a data-availability confidence tier to each city, based on the completeness of the NBS inventory, the availability of locally validated reference data, and the OSM contributor density for the building model. Cross-city comparisons will report these tiers alongside the analytical results so that readers can assess the relative reliability of findings across cities.

7.2.5. Mitigation of NBS Classification Inconsistency

Inconsistent NBS classification across cities introduces thematic uncertainty primarily into three analyses: (i) land cover-derived NBS fractions (WorldCover classes, CLCplus categories, imperviousness/greenness fraction at 10 m); (ii) the NBS inventory used for local attribution in the cross-city statistical analysis; and (iii) the LCZ-stratified thermal contrast analysis, where the assignment of vegetation-dominated pixels to LCZ classes A–G depends on consistent thematic definitions.

To quantify this uncertainty, NBS classification sensitivity tests will be conducted by applying alternative thematic mappings, drawn from the EU NBS taxonomy, the IUCN-based classification, and local planning frameworks to a representative subset of cities. The resulting variation in NBS fraction estimates and LCZ-level LST contrasts will be reported as an uncertainty range. Disagreement rates between the harmonized typology and local inventories will also be documented per city.

To reduce this uncertainty, a harmonized four-class NBS typology will be adopted across all local-study cities: (i) large urban parks and forests; (ii) smaller green spaces, street trees, and urban greenery; (iii) blue infrastructure including rivers, retention ponds, and stormwater management features; and (iv) hybrid blue-green elements. Each class will be mapped using the most spatially appropriate available product, WorldCover 10 m or CLCplus for broad categories, the high-

resolution imperviousness/greenness layer for fine-scale differentiation, and cross-validated against stakeholder inventories where available.

Residual classification uncertainty will be reported for each city as described in Section 7.2.3.

7.2.6. Mitigation of EO Data Availability Gaps

For cities where ancillary EO data coverage is incomplete or less reliable, for example for Kigali and Manila, an alternative data strategy will be implemented. Where LoD1 building height data from WSF 4D are incomplete, a trained deep learning model will be used to predict building height at 10 m resolution using Sentinel-2 and Sentinel-1 inputs, conditioned on the input data available in the area for the NBS evaluation time frame. WSF 4D gaps and OSM tagging quality metrics will be documented per city, providing users the ready to analyse outputs with explicit information on data completeness. For cities where fallback strategies cannot fully compensate for coverage gaps, results will be assigned to the lower attribution confidence tier and interpreted with additional caution in cross-city comparisons.

The combined effect of the alternative data strategy and the attribution confidence reporting system is to ensure that data availability uncertainty is fully transparent and traceable in the analytical outputs. This approach accepts that uneven analytical depth across cities is an inherent feature of a globally representative study and manages it through explicit documentation rather than through artificial equalization of data quality.

8. Conclusions

The results of the activities carried out in WP2, reported in the previous sections, are two sets of studies ready to be performed at the global level on 159 cities and at the local level on a subset of 10 cities. The criteria for the selection of the city, the ECVs that will be considered, the additional data sets that have been collected and tailored for the two studies, as well as some preliminary examples of the studies show that the project team is ready to transition to the third task of the projects, i.e., the realization of the scientific studies at the two selected geographical scales, aiming at providing an answer to the scientific questions of the MOMO-NBS project:

- How does climate change affect cities with different morphologies, from regional to global level?
- To what extent can existing ECVs be used to assess the effects of NBS on urban climate at the urban area level?

- How can new data on 3D city morphology and green/grey infrastructure be linked with ECVs to effectively support local NBS implementation for climate change adaptation?

9. References

Burgess, E., The growth of the city: an introduction to a research project. JM Marzluff (Ed.), The city, University of Chicago Press, Boston, MA (1925), pp. 71-78

Che, Y., Li, X., Liu, X., Wang, Y., Liao, W., Zheng, X., Zhang, X., Xu, X., Shi, Q., Zhu, J., Zhang, H., Yuan, H., and Dai, Y.: 3D-GloBFP: the first global three-dimensional building footprint dataset, Earth Syst. Sci. Data, 16, 5357–5374, https://doi.org/10.5194/essd-16-5357-2024.

Demuzere, M., Bechtel, B., Middel, A., Mills G., LCZ map https://doi.org/10.6084/m9.figshare.13322450 (2020), Accessed 16th Apr 2026

Erbertseder, T., Taubenböck, H., Esch, T., Gilardi, L., Paeth, H. and S. Dech: NO2 pollution trends and settlement growth in megacities, Journal of Selected Topics in Applied Earth Observations and Remote Sensing, vol. 17, 2024, doi: 10.1109/JSTARS.2024.3419573.

Erbertseder, T., Baier, F., & Bergemann, C. (2015). Der Wochenrhythmus der Städte. In H. Taubenböck, M. Wurm, P. Esch, & S. Dech (Eds.), Globale Urbanisierung: Perspektive aus dem All (pp. 151–158). Springer. https://doi.org/10.1007/978-3-662-44841-0

Esch, T., Brzoska, E., Dech, S., Leutner, B., Palacios-Lopez, D., Metz-Marconcini, A., Marconcini, M., Roth, A., Zeidler, J.: World Settlement Footprint 3D - A first three-dimensional survey of the global building stock. Remote Sensing of Environment, Volume 270, 2022, 112877, ISSN 0034-4257. https://doi.org/10.1016/j.rse.2021.112877.

Esch, T., Deininger, K., Hilhorst, T., Kacholia, D., Marconcini, M., Zeidler, J., Zygar, C.: World Settlement Footprint 4D – Integrating Height, Volume, and Construction Period into Global Building Footprints. Scientific Data. Submitted in April 2026.

Florczyk A.J., Corbane C., Ehrlich D., Freire S., Kemper T., Maffenini L., Melchiorri M., Pesaresi M., Politis P., Schiavina M., Sabo F., Zanchetta L.: GHSL Data Package 2019, EUR 29788 EN, Publications Office of the European Union, Luxembourg, 2019, ISBN 978-92-76-13186-1, doi:10.2760/290498, JRC 117104.

Iungman, T., Khomenko, S., Pereira Barboza, E., Cirach, M., Gonçalves, K., Petrone, P., Erbertseder, T., Taubenböck, H., Chakraborty, T. and M. Nieuwenhuijsen, The impact of urban configuration types on urban heat islands, air pollution, CO2 emissions, and mortality in Europe: a data science approach, The Lancet Planetary Health, Volume 8, Issue 7, 2024, https://doi.org/10.1016/S2542-5196(24)00120-7.

JRC, 2026. World Human Settlement Layer: https://human-settlement.emergency.copernicus.eu/download.php?ds=ucdb

Lloyd, S. P., Least Squares Quantization in PCM, IEEE Trans. Inf. Theory, vol. 28, pp. 129–137, 1982, doi: 10.1109/TIT.1982.1056489.

Marconcini, M., Metz-Marconcini, A., Üreyen, S., Palacios-Lopez, D., Hanke, W., Bachofer, F., Zeidler, J., Esch, T., Gorelick, N., Kakarla, A.: Outlining where humans live - the world settlement footprint 2015. Sci. Data 7, 2020, 1–14. https://doi.org/10.1038/s41597-020-00580-5.

Marconcini, M., Metz-Marconcini, A., Esch, T., Gorelick, N.: Understanding Current Trends in Global Urbanisation – the World Settlement Footprint suite. GI Forum 2021, 5-8 July 2021, Salzburg, Austria. https://dx.doi.org/10.1553/GISCIENCE2021_01_S33.4

McInnes, L., Healy, J., Melville J.,UMAP: Uniform Manifold Approximation and Projection for Dimension Reduction https://umap-learn.readthedocs.io/en/latest/index.html, (2018), Accessed 16th April 2026

Melchiorri, M., Mari Rivero, I., Florio, P., Schiavina, M., Krasnodebska, K., Politis, P., Uhl, J., Pesaresi, M., Maffenini, L., Sulis, P., Crippa, M., Guizzardi, D., Pisoni, E., Belis, C., Oom, D., Branco, A., Mwaniki, D., Githira, D., Kochulem, E., Tommasi, P., Carioli, A., Ehrlich, D., Kemper, T. and Dijkstra, L.: Stats in the City – the GHSL Urban Centre Database 2025. European Commission, Joint Research Centre, Publications Office of the European Union, Luxembourg, 2024, https://data.europa.eu/doi/10.2760/3046391, JRC139768.

Müller, I., Erbertseder, T. and Taubenböck, H.: Tropospheric NO2: Explorative Analyses of Spatial Variability and Impact Factors, Rem. Sens. Env., Volume 270, 112839, https://doi.org/10.1016/j.rse.2021.112839, 2022.

Oostwegel, L.J.N., Schorlemmer, D. & Guéguen, P. From Footprints to Functions: A Comprehensive Global and Semantic Building Footprint Dataset. Sci Data 12, 1699 (2025): https://doi.org/10.1038/s41597-025-06132-z.

OpenStreetMap contributors Nominatim https://nominatim.openstreetmap.org/ui/search.html (2015), Accessed 16th April Jan 2026

Overture Maps Foundation, 2026: Buildings data. https://docs.overturemaps.org/

Pesaresi, M., Schiavina, M., Politis, P., Freire, S., Krasnodębska, K., Uhl, J. H.,Kemper, T., 2024: Advances on the Global Human Settlement Layer by joint assessment of Earth Observation and population survey data. International Journal of Digital Earth, 17(1). https://doi.org/10.1080/17538947.2024.2390454.

Schiavina M., Melchiorri M., Pesaresi M.: GHS-SMOD R2023A - GHS settlement layers, application of the Degree of Urbanisation methodology (stage I) to GHS-POP R2023A and GHS-BUILT-S R2023A, multitemporal (1975-2030). European Commission, Joint Research Centre (JRC), 2023. PID: http://data.europa.eu/89h/a0df7a6f-49de-46ea-9bde-563437a6e2ba, doi:10.2905/A0DF7A6F-49DE-46EA-9BDE-563437A6E2BA

Sirko, W., Asiedu Brempong, E., Marcos, J.T.C., Annkah, A., Korme, A., Alewi Hassen, M., Sapkota, K., Shekel, T., Diack, A., Nevo, S., Hickey, J., Quinn, J., 2024: High-Resolution Building and Road Detection from Sentinel-2. https://doi.org/10.48550/arXiv.2310.11622.

Stewart, I. D. Oke, T. E., Local climate zones for urban temperature studies, Bull Am Meteorol Soc, 93 (2012), pp. 1879-1900, 2020.

Taubenböck, H., Debray, H., Qiu, C., Schmitt, M., Wang, Y., Zhu, X.X: Seven city types representing morphologic configurations of cities across the globe. *Cities*, Volume 105, 2020. https://doi.org/10.1016/j.cities.2020.102814.

Thorndike, R. L., Who belongs in the family? Psychometrika, vol. 18, pp. 267–276, 1953, doi: 10.1007/BF02289263.

ANNEX I

Tab. A.1: List of 159 cities used for global study.

CITY	COUNTRY	CITY AREA* [km^2]	CLIMATE ZONE **	POPULATION*	MORPHOLOGY ***
Abidjan	Côte d'Ivoire	503	Tropical monsoon	6,450,316	Low structural variability, medium compact, low-rise, medium shares of open space
Abu Dhabi	United Arab Emirates	107	Hot desert	508,976	High structural variability, medium compact, low-rise, very high shares of non-built space
Abuja	Nigeria	319	Tropical savanna	1,322,229	Medium structural variability, low compact, low-rise, high shares of non-built space
Accra	Ghana	1121	Tropical savanna	5,890,466	Medium structural variability, low compact, low-rise, high shares of non-built space
Addis Ababa	Ethiopia	465	Subtropical highland (dry winter, warm summer)	7,280,463	High structural variability, medium compact, mid-rise, medium shares of open space
Ahmedabad	India	365	Hot semi-arid (steppe)	7,898,650	Low structural variability, medium compact, low-rise, medium shares of open space
Al Ain	United Arab Emirates	206	Hot desert	672,213	High structural variability, medium compact, low-rise, very high shares of non-built space
Amsterdam	Netherlands	308	Oceanic	1,223,407	High structural variability, medium compact, mid-rise, medium shares of open space
Antananarivo	Madagascar	442	Subtropical highland (dry winter, warm summer)	4,255,254	High structural variability, low compact, low-rise, medium shares of open space
Asmara	Eritrea	43	Hot semi-arid (steppe)	251,980	High structural variability, medium compact, low-rise, very high shares of non-built space
Athens	Greece	412	Hot-summer Mediterranean	3,166,757	High structural variability, medium compact, mid-rise, medium shares of open space
Atlanta	United States	292	Humid subtropical	602,708	High structural variability, low compact, low-rise, medium shares of open space

Baghdad	Iraq	688	Hot desert	6,891,722	Low structural variability, medium compact, low-rise, medium shares of open space
Bamako	Mali	407	Hot semi-arid (steppe)	3,960,563	Medium structural variability, low compact, low-rise, high shares of non-built space
Bandung	Indonesia	988	Tropical rainforest	8,691,181	Medium structural variability, medium compact, low-rise, medium shares of open space
Bangkok	Thailand	2697	Tropical savanna	19,048,032	Low structural variability, medium compact, mid-rise, lowest shares of open space
Barcelona	Spain	438	Hot-summer Mediterranean	3,908,362	High structural variability, medium compact, mid-rise, medium shares of open space
Beijing	China	2179	Humid continental (dry winter, hot summer)	18,150,576	Medium structural variability, medium compact, low-rise, medium shares of open space
Bengaluru	India	1008	Tropical savanna	15,178,533	Low structural variability, medium compact, low-rise, medium shares of open space
Berlin	Germany	681	Oceanic	3,549,997	High structural variability, medium compact, mid-rise, medium shares of open space
Blantyre	Malawi	191	Tropical savanna	941,888	High structural variability, low compact, low-rise, medium shares of open space
Bogota	Colombia	534	Oceanic / temperate highland	10,419,361	Medium structural variability, medium compact, low-rise, medium shares of open space
Brisbane	Australia	701	Humid subtropical	1,359,105	High structural variability, low compact, low-rise, medium shares of open space
Brussels	Belgium	235	Oceanic	1,468,754	High structural variability, medium compact, mid-rise, medium shares of open space
Bucharest	Romania	260	Humid continental (warm summer)	1,971,350	Low structural variability, medium compact, low-rise, medium shares of open space
Budapest	Hungary	368	Oceanic / temperate	1,743,875	High structural variability, medium compact, mid-rise, medium shares of open space
Buenos Aires	Argentina	2186	Humid subtropical	14,179,912	Medium structural variability, medium compact, low-rise, medium shares of open space

Bujumbura	Burundi	141	Tropical savanna	1,403,419	Medium structural variability, low compact, low-rise, high shares of non-built space
Córdoba	Spain	32	Hot-summer Mediterranean	239,916	Medium structural variability, medium compact, low-rise, medium shares of open space
Cairo	Egypt	1680	Hot desert	25,230,325	High structural variability, medium compact, low-rise, very high shares of non-built space
Calgary	Canada	533	Humid continental (warm summer)	1,524,649	High structural variability, low compact, low-rise, medium shares of open space
Cape Town	South Africa	695	Warm-summer Mediterranean	4,338,251	Low structural variability, medium compact, low-rise, medium shares of open space
Cebu City	Philippines	416	Tropical savanna	3,191,585	High structural variability, low compact, low-rise, medium shares of open space
Changsha	China	423	Humid subtropical	3,246,971	High structural variability, medium compact, mid-rise, medium shares of open space
Chattogram	Bangladesh	519	Tropical monsoon	5,175,717	High structural variability, medium compact, mid-rise, medium shares of open space
Chennai	India	1052	Tropical savanna	11,466,400	Low structural variability, medium compact, low-rise, medium shares of open space
Chicago	United States	2046	Humid continental (hot summer)	5,318,735	Medium structural variability, medium compact, low-rise, medium shares of open space
Chongqing	China	653	Humid subtropical	8,449,690	High structural variability, medium compact, mid-rise, medium shares of open space
Dakar	Senegal	277	Hot semi-arid (steppe)	3,970,202	High structural variability, medium compact, low-rise, very high shares of non-built space
Dar es-Salaam	Tanzania	907	Tropical savanna	8,918,525	High structural variability, low compact, low-rise, medium shares of open space
Denver	United States	1194	Cold semi-arid (steppe)	2,425,086	High structural variability, low compact, low-rise, medium shares of open space
Dhaka	Bangladesh	6611	Tropical savanna	37,307,160	High structural variability, medium compact, mid-rise, medium shares of open space

Douala	Cameroon	280	Tropical monsoon	4,457,862	Low structural variability, medium compact, low-rise, medium shares of open space
Dubai	United Arab Emirates	854	Hot desert	4,565,478	High structural variability, medium compact, low-rise, very high shares of non-built space
Dublin	Ireland	301	Oceanic	1,124,520	High structural variability, medium compact, mid-rise, medium shares of open space
Faisalabad	Pakistan	326	Hot semi-arid (steppe)	5,676,793	High structural variability, medium compact, low-rise, very high shares of non-built space
Fortaleza	Brazil	413	Tropical savanna (dry summer)	3,324,149	Low structural variability, medium compact, low-rise, medium shares of open space
General Santos	Philippines	103	Tropical monsoon	470,212	High structural variability, low compact, low-rise, medium shares of open space
Guadalajara	Mexico	598	Tropical savanna	4,138,350	Medium structural variability, medium compact, low-rise, medium shares of open space
Guangzhou	China	6454	Humid subtropical (dry winter)	42,987,704	Low structural variability, medium compact, mid-rise, lowest shares of open space
Hamburg	Germany	478	Oceanic	1,733,898	High structural variability, medium compact, mid-rise, medium shares of open space
Hanoi	Vietnam	925	Humid subtropical (dry winter)	4,965,520	Low structural variability, medium compact, low-rise, medium shares of open space
Harare	Zimbabwe	603	Subtropical highland (dry winter, warm summer)	2,076,037	High structural variability, low compact, low-rise, medium shares of open space
Hargeisa	Somalia	84	Hot semi-arid (steppe)	1,500,449	High structural variability, medium compact, low-rise, very high shares of non-built space
Ho Chi Minh City	Vietnam	1487	Tropical savanna	14,557,830	Low structural variability, medium compact, low-rise, medium shares of open space
Hong Kong	China	220	Humid subtropical (dry winter)	4,807,599	High structural variability, low compact, low-rise, medium shares of open space
Houston	United States	1859	Humid subtropical	4,301,461	High structural variability, low compact, low-rise, medium shares of open space

Hyderabad	India	889	Hot semi-arid (steppe)	9,455,230	Low structural variability, medium compact, low-rise, medium shares of open space
Islamabad	Pakistan	550	Humid subtropical	4,913,528	High structural variability, low compact, low-rise, medium shares of open space
Istanbul	Turkey	1269	Hot-summer Mediterranean	14,210,222	High structural variability, medium compact, mid-rise, medium shares of open space
Izmir	Turkey	307	Hot-summer Mediterranean	2,457,529	High structural variability, medium compact, mid-rise, medium shares of open space
Jaipur	India	458	Hot semi-arid (steppe)	4,229,050	Low structural variability, medium compact, low-rise, medium shares of open space
Jakarta	Indonesia	4614	Tropical savanna	40,545,126	Medium structural variability, medium compact, low-rise, medium shares of open space
Johannesburg	South Africa	1756	Subtropical highland (dry winter, warm summer)	8,592,843	Low structural variability, medium compact, low-rise, medium shares of open space
Kabul	Afghanistan	371	Cold semi-arid (steppe)	6,254,679	High structural variability, medium compact, low-rise, very high shares of non-built space
Kampala	Uganda	810	Tropical rainforest	5,177,878	Medium structural variability, low compact, low-rise, high shares of non-built space
Kano	Nigeria	419	Hot semi-arid (steppe)	5,110,616	Medium structural variability, low compact, low-rise, high shares of non-built space
Karachi	Pakistan	834	Hot desert	21,031,703	High structural variability, medium compact, low-rise, very high shares of non-built space
Kathmandu	Nepal	350	Subtropical highland (dry winter, warm summer)	3,862,697	High structural variability, low compact, low-rise, medium shares of open space
Khartoum	Sudan	958	Hot desert	7,114,789	High structural variability, medium compact, low-rise, very high shares of non-built space
Kigali	Rwanda	286	Oceanic / subtropical highland	1,621,760	Medium structural variability, low compact, low-rise, high shares of non-built space
Kinshasa	Democratic Republic of the Congo	487	Tropical savanna	12,945,683	Medium structural variability, low compact, low-rise, high shares of non-built space

Kitwe	Zambia	117	Tropical savanna	731,813	High structural variability, low compact, low-rise, medium shares of open space
Kolkata	India	2482	Tropical savanna	23,314,585	High structural variability, low compact, low-rise, medium shares of open space
Kozhikode	India	1341	Tropical monsoon	7,612,130	High structural variability, low compact, low-rise, medium shares of open space
Kuala Lumpur	Malaysia	1340	Tropical rainforest	8,413,206	Medium structural variability, medium compact, low-rise, medium shares of open space
Kumasi	Ghana	469	Tropical savanna	4,923,115	Medium structural variability, low compact, low-rise, high shares of non-built space
Kyiv	Ukraine	410	Humid continental (warm summer)	2,575,199	High structural variability, medium compact, mid-rise, medium shares of open space
La Paz	Bolivia	291	Subtropical highland (dry winter, warm summer)	2,063,633	High structural variability, low compact, low-rise, medium shares of open space
Lagos	Nigeria	1199	Tropical monsoon	12,846,045	Low structural variability, medium compact, low-rise, medium shares of open space
Lahore	Pakistan	898	Hot semi-arid (steppe)	14,305,060	Low structural variability, medium compact, low-rise, medium shares of open space
Las Vegas	United States	851	Hot desert	2,371,780	High structural variability, low compact, low-rise, medium shares of open space
Lhasa	China	75	Cold semi-arid (steppe)	273,179	High structural variability, medium compact, low-rise, very high shares of non-built space
Lilongwe	Malawi	136	Tropical savanna	1,018,798	Medium structural variability, low compact, low-rise, high shares of non-built space
Lima	Peru	984	Cold coastal desert	10,828,104	Low structural variability, medium compact, low-rise, medium shares of open space
Lisbon	Portugal	426	Hot-summer Mediterranean	1,974,574	High structural variability, medium compact, mid-rise, medium shares of open space
London	United Kingdom	1649	Oceanic	10,408,332	High structural variability, medium compact, mid-rise, medium shares of open space

Los Angeles	United States	4498	Warm-summer Mediterranean	13,474,333	Low structural variability, medium compact, mid-rise, lowest shares of open space
Lucknow	India	513	Hot semi-arid (steppe)	5,214,964	Low structural variability, medium compact, low-rise, medium shares of open space
Lusaka	Zambia	360	Tropical savanna	3,658,064	High structural variability, low compact, low-rise, medium shares of open space
Madrid	Spain	680	Hot-summer Mediterranean	5,680,137	High structural variability, medium compact, mid-rise, medium shares of open space
Manchester	United Kingdom	751	Oceanic	2,539,907	High structural variability, medium compact, mid-rise, medium shares of open space
Manila	Philippines	2555	Tropical savanna	25,921,189	Medium structural variability, medium compact, low-rise, medium shares of open space
Maputo	Mozambique	570	Hot semi-arid (steppe)	3,533,370	High structural variability, low compact, low-rise, medium shares of open space
Marseille	France	185	Hot-summer Mediterranean	911,934	High structural variability, medium compact, mid-rise, medium shares of open space
Medan	Indonesia	607	Tropical rainforest	4,350,624	Medium structural variability, medium compact, low-rise, medium shares of open space
Melbourne	Australia	1611	Oceanic	4,010,658	Medium structural variability, medium compact, low-rise, medium shares of open space
Mexico City	Mexico	2134	Subtropical highland (dry winter, warm summer)	17,639,164	Medium structural variability, medium compact, low-rise, medium shares of open space
Miami	United States	2784	Tropical savanna	5,733,042	Medium structural variability, medium compact, low-rise, medium shares of open space
Milan	Italy	785	Humid subtropical	3,135,553	High structural variability, medium compact, mid-rise, medium shares of open space
Minneapolis [Saint Paul]	United States	611	Humid continental (warm summer)	1,217,972	Medium structural variability, medium compact, low-rise, medium shares of open space
Minsk	Belarus	245	Humid continental (warm summer)	2,093,512	High structural variability, medium compact, mid-rise, medium shares of open space

Mogadishu	Somalia	186	Hot desert	4,798,453	Low structural variability, medium compact, low-rise, medium shares of open space
Mombasa	Kenya	181	Tropical savanna	1,617,739	Low structural variability, medium compact, low-rise, medium shares of open space
Monterrey	Mexico	685	Hot semi-arid (steppe)	4,011,151	Medium structural variability, medium compact, low-rise, medium shares of open space
Moscow	Russia	1545	Humid continental (warm summer)	14,384,082	High structural variability, medium compact, mid-rise, medium shares of open space
Mumbai	India	738	Tropical savanna	20,453,270	High structural variability, medium compact, mid-rise, medium shares of open space
Munich	Germany	345	Oceanic	1,827,704	High structural variability, medium compact, mid-rise, medium shares of open space
Muscat	Oman	148	Hot desert	734,542	High structural variability, medium compact, low-rise, very high shares of non-built space
Mwanza	Tanzania	175	Tropical savanna	977,475	High structural variability, low compact, low-rise, medium shares of open space
Nairobi	Kenya	598	Subtropical highland (dry winter, warm summer)	6,646,257	High structural variability, low compact, low-rise, medium shares of open space
Nanjing	China	1012	Humid subtropical	8,061,029	High structural variability, low compact, low-rise, medium shares of open space
New Delhi	India	2139	Hot semi-arid (steppe)	31,422,508	Low structural variability, medium compact, low-rise, medium shares of open space
New York City	United States	3031	Humid subtropical	14,197,659	Medium structural variability, medium compact, low-rise, medium shares of open space
Osaka	Japan	2212	Humid subtropical	12,653,994	Medium structural variability, medium compact, low-rise, medium shares of open space
Oslo	Norway	244	Humid continental (warm summer)	889,573	High structural variability, medium compact, mid-rise, medium shares of open space
Ouagadougou	Burkina Faso	495	Hot semi-arid (steppe)	3,616,268	High structural variability, medium compact, low-rise, very high shares of non-built space

Paris	France	1421	Oceanic	9,328,385	High structural variability, medium compact, mid-rise, medium shares of open space
Perth	Australia	784	Hot-summer Mediterranean	1,357,382	High structural variability, low compact, low-rise, medium shares of open space
Philadelphia	United States	654	Humid subtropical	2,286,396	Medium structural variability, medium compact, low-rise, medium shares of open space
Phnom Penh	Cambodia	354	Tropical savanna	2,419,131	High structural variability, low compact, low-rise, medium shares of open space
Phoenix	United States	1304	Hot desert	2,608,874	High structural variability, low compact, low-rise, medium shares of open space
Port Harcourt	Nigeria	310	Tropical monsoon	2,623,780	Low structural variability, medium compact, low-rise, medium shares of open space
Port Moresby	Papua New Guinea	72	Tropical savanna	442,165	Medium structural variability, low compact, low-rise, high shares of non-built space
Port-au-Prince	Haiti	275	Tropical savanna	1,733,378	High structural variability, low compact, low-rise, medium shares of open space
Prague	Czechia	263	Oceanic	1,201,278	High structural variability, medium compact, mid-rise, medium shares of open space
Pune	India	580	Hot semi-arid (steppe)	6,674,000	Medium structural variability, low compact, low-rise, high shares of non-built space
Quito	Ecuador	380	Oceanic / subtropical highland	2,605,678	High structural variability, low compact, low-rise, medium shares of open space
Rio de Janeiro	Brazil	1285	Tropical savanna	9,853,693	Medium structural variability, medium compact, low-rise, medium shares of open space
Riyadh	Saudi Arabia	1108	Hot desert	7,970,319	Medium structural variability, medium compact, low-rise, medium shares of open space
Rome	Italy	467	Hot-summer Mediterranean	2,476,089	High structural variability, medium compact, mid-rise, medium shares of open space
São Paulo	Brazil	2111	Oceanic / humid subtropical	19,485,158	Medium structural variability, medium compact, low-rise, medium shares of open space

Saint Petersburg	Russia	550	Humid continental (warm summer)	4,878,966	High structural variability, medium compact, mid-rise, medium shares of open space
San Francisco	United States	1614	Warm-summer Mediterranean	4,718,349	Medium structural variability, medium compact, low-rise, medium shares of open space
Santiago	Chile	801	Warm-summer Mediterranean	6,633,767	Low structural variability, medium compact, low-rise, medium shares of open space
Seattle	United States	1123	Oceanic	2,099,643	Medium structural variability, medium compact, low-rise, medium shares of open space
Seoul	South Korea	2282	Humid continental (dry winter, hot summer)	22,261,692	Medium structural variability, medium compact, low-rise, medium shares of open space
Shanghai	China	3128	Humid subtropical	30,678,616	Low structural variability, medium compact, mid-rise, lowest shares of open space
Singapore	Singapore	438	Tropical rainforest	5,117,759	Medium structural variability, medium compact, low-rise, medium shares of open space
Stockholm	Sweden	339	Humid continental (warm summer)	1,543,892	High structural variability, medium compact, mid-rise, medium shares of open space
Surabaya	Indonesia	1304	Tropical savanna	6,856,993	Medium structural variability, medium compact, low-rise, medium shares of open space
Surat	India	296	Hot semi-arid (steppe)	7,100,723	Medium structural variability, low compact, low-rise, high shares of non-built space
Sydney	Australia	1378	Humid subtropical	4,375,395	High structural variability, low compact, low-rise, medium shares of open space
Taipei	Taiwan	972	Humid subtropical	9,686,521	Medium structural variability, medium compact, low-rise, medium shares of open space
Tashkent	Uzbekistan	598	Cold semi-arid (steppe)	3,874,653	High structural variability, medium compact, mid-rise, medium shares of open space
Tehran	Iran	825	Cold semi-arid (steppe)	9,363,124	High structural variability, medium compact, low-rise, very high shares of non-built space
Tel Aviv	Israel	333	Hot-summer Mediterranean	2,628,335	High structural variability, medium compact, mid-rise, medium shares of open space

Tianjin	China	671	Humid continental (dry winter, hot summer)	7,330,648	Low structural variability, medium compact, low-rise, medium shares of open space
Tokyo	Japan	5165	Humid subtropical	33,155,907	Low structural variability, medium compact, mid-rise, lowest shares of open space
Toronto	Canada	1620	Humid continental (warm summer)	5,566,382	Medium structural variability, medium compact, low-rise, medium shares of open space
Toulon	France	111	Hot-summer Mediterranean	290,434	High structural variability, medium compact, mid-rise, medium shares of open space
Vancouver	Canada	649	Oceanic	2,198,107	High structural variability, medium compact, mid-rise, medium shares of open space
Vienna	Austria	325	Oceanic	2,056,565	High structural variability, medium compact, mid-rise, medium shares of open space
Wellington	New Zealand	64	Oceanic	154,120	High structural variability, low compact, low-rise, medium shares of open space
Wuhan	China	772	Humid subtropical	8,079,484	High structural variability, medium compact, mid-rise, medium shares of open space
Yangon	Myanmar	545	Tropical monsoon	6,190,958	High structural variability, low compact, low-rise, medium shares of open space
Zanzibar City	Tanzania	121	Tropical rainforest	1,026,755	High structural variability, low compact, low-rise, medium shares of open space
Zurich	Switzerland	187	Oceanic	689,208	High structural variability, medium compact, mid-rise, medium shares of open space

* The city area and population are sourced from GHS-UCDB R2024A.
** The cities are categorized based on the Köppen-Geiger climate classification.
*** The city morphology follows the categorization introduced by Taubenböck et al. (2020).